

Document downloaded from:

<http://hdl.handle.net/10251/153467>

This paper must be cited as:

Li, C.; Moliner Marin, M.; Corma Canós, A. (2018). Building zeolites from precrystallized units: nanoscale architecture. *Angewandte Chemie International Edition*. 57(47):15330-15353. <https://doi.org/10.1002/anie.201711422>



The final publication is available at

<https://doi.org/10.1002/anie.201711422>

Copyright John Wiley & Sons

Additional Information

This is the peer reviewed version of the following article: Angew. Chem. Int. Ed. 2018, 57, 15330–15353, which has been published in final form at <https://doi.org/10.1002/anie.201711422>. This article may be used for non-commercial purposes in accordance with Wiley Terms and Conditions for Self-Archiving.

Building zeolites from pre-crystallized units: nanoscale architecture

Chengeng Li, Manuel Moliner,* Avelino Corma*

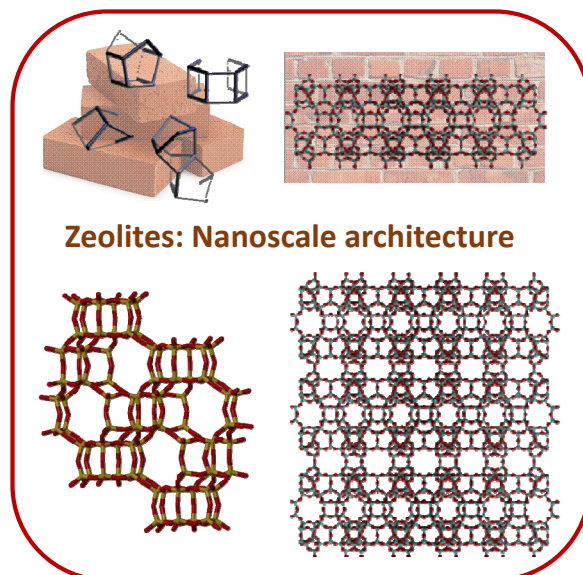
Instituto de Tecnología Química, Universitat Politècnica de València-Consejo
Superior de Investigaciones Científicas, Avenida de los Naranjos s/n, 46022 València,
Spain

*Corresponding authors: E-mail addresses: acorma@itq.upv.es;
mmoliner@itq.upv.es

Abstract

playText><earlier descriptions by Barrer in the 40's on converting natural minerals into synthetic zeolites, the use of pre-crystallized zeolites as crucial inorganic directing agents to synthesize other crystalline zeolites with improved physico-chemical properties, has become a very intense and relevant research field, allowing the design, particularly in the recent years, of new industrial catalysts. In the present review, we will highlight how the presence of some crystalline fragments in the synthesis media, such as small secondary building units (SBUs) or layered substructures, not only favors the crystallization of other zeolites presenting similar SBUs or layers, but also permits mostly controlling important parameters affecting to their catalytic activity (i.e. chemical composition, crystal size, or porosity, among others). In this sense, the recent advances on the preparation of 3-D and 2-D related zeolites through seeding and zeolite-to-zeolite transformation processes will be extensively revised, including their preparation in presence or absence of organic structure directing agents (OSDAs), with the aim of introducing general guidelines for designing more efficient future synthesis approaches for target zeolites.

2



1.- Introduction

Zeolites are crystalline microporous materials with uniform channel systems and molecular-sized pore windows (1). They are widely used as catalysts and adsorbents in a variety of industrial processes, including oil refining, petrochemical and fine chemical processes, and detergents (2, 3). The zeolite structures are formed by TO_4 tetrahedral units ($\text{T}=\text{Si, Al, P, etc.}$) that are connected creating different secondary building blocks (SBUs) and, those finally connected to form thorough frameworks.

Although more than 220 different zeolite crystalline structures have been discovered (4), the synthesis mechanisms comprising zeolite nucleation and crystallization involve many time-dependent chemical processes that take place in multiple phases (1, 5-9) and, consequently, the under demand crystallization of a specific zeolite structure is still far from being achieved (10). Nevertheless, based on semiempirical routes it is possible for scientists to conduct synthesis towards zeolite frameworks with particular physico-chemical properties, such as for instance, pore topologies or crystal sizes (11-13). Recently, another research front has been opened with the “ab-initio” synthesis of zeolites for pre-established catalytic applications (14).

The introduction of organic cations has greatly expanded the possibilities in zeolite synthesis, and many efforts have been devoted to design families of organic molecules as organic structure directing agents (OSDAs) (15-17). Most of those molecules are amines and ammonium cations (18), phosphonium or phosphazenes (19, 20), and their properties, including shape, size or flexibility, have an important effect on the pore topology and the framework composition of the resultant zeolite (16, 17).

Besides OSDAs, the presence of particular heteroatoms in framework positions could not only introduce catalytic or cation-exchange sites, but also act as inorganic SDAs in zeolite synthesis (1, 5). In fact, heteroatoms, different in charge and atomic diameter compared to silicon, provide possibility to have unusual ways of TO_4 connection and form different SBUs (5). Introducing germanium, for example, has made possible the formation of abundant $d4r$ and $d3r$ units in the synthesis gel (21). Researchers from ITQ have proven that introducing Ge in synthesis gel could lead to the formation of a series of new zeolite structures with lower

framework-densities (FD) and larger pore dimensions (22-24).

Beyond these single inorganic atoms and organic molecules for designing new or improved zeolite structures, the use of zeolites as a source of Si and Al to synthesize other zeolites has recently gained attention in the literature (25-29). In general, it has been described that well-formed zeolite precursors would decompose into small fragments containing characteristic SBUs in the synthesis gel when hydrothermally treated, favoring the rearrangement and crystallization of other structures sharing similar SBUs (30-32). Researchers have succeeded in the hydrothermal transformation of some crystalline zeolites, i.e. FAU, into many other structures, such as CHA, LEV and AEI, among others, by combining the use of the pre-crystallized zeolites and different OSDA molecules (33-36). These zeolite-to-zeolite transformations allow controlling the particle sizes, heteroatom substitutions, or solid yields of different zeolites that were not adjusted by using other amorphous bulk silica sources (28, 29, 36, 37). In a very illustrative work in 1995, Zones and Nakagawa described that the use of modified zeolites as reagents in zeolite synthesis would address nucleation selectivity based on the “goodness-of-fit” for nuclei that resemble the final crystalline product, resulting in more efficient nucleation rates towards specific zeolites (38).

Interestingly, this zeolite-to-zeolite transformation can be extended to the synthesis of new zeolite structures through condensation/expansion of layered zeolite precursors (39, 40), and to the synthesis of OSDA-free zeolites (41, 42). On the one hand, the transformation of layered zeolite precursors into 3-D or 2-D crystalline zeolites allows either synthesizing new crystalline zeolite structures through topotactic transformations or increasing the accessibility of acid sites within industrially-relevant zeolite catalysts. On the other hand, attempts to efficiently design high-silica zeolites through OSDA-free methodologies have been preferentially undergone using pre-crystallized zeolites as full raw materials (42) or as zeolite crystal seeds (41), as a solution for costs and environmental issues during zeolite production caused by usage of OSDA. In both cases, it has been shown that the presence of specific SBUs on the pre-crystallized zeolites favors formation of zeolites containing SBUs in common.

It is noteworthy that the structural transformation of crystalline materials into zeolites was already envisioned by Barrer in the 40's when converting natural minerals into zeolites

(43-45). Nevertheless, the modern technologies and present knowledge enable researchers to combine this traditional technique with assistance of OSDAs and/or new structural modification methods.

In this manuscript, the recent progresses of interzeolite transformations in zeolite synthesis have been deeply revised, focusing on the inorganic directing roles of the pre-crystallized zeolites during the nucleation and crystallization processes. Mechanistic explanations for the experimental observations were presented as well. Nevertheless, limited by state-of-art techniques to identify the SBUs with sub-atomic scale of size, some of the mechanisms presented remain under debate. For this reason, both the certainty and the uncertainty of those mechanistic explanations are provided, with the aim of introducing some guidelines for designing more efficient future synthesis approaches for target zeolites.

2.- Proposed mechanisms for the interzeolite transformations

2.1.- Interzeolite transformations under OSDA-free conditions

2.1.1.- Former mechanisms

Barrer first studied the effect of the concentration of the hydroxyl anions in the transformation of zeolite A into other crystalline phases without using OSDA molecules (46). In this former study, it was observed that the concentration of NaOH could alter synthesis toward a hydroxysodalite dense phase or zeolite P (GIS topology) (46). The author suggested that the nucleation and crystal growth may occur at the surface of the former zeolite A, indicating a direct solid-solid transformation process (46). However, the first systematic mechanistic study to understand the interzeolite transformations were carried out by Subotic et al. twenty years later (47, 48), when the transformation of zeolite A into the dense hydroxysodalite phase was evaluated under alkaline conditions (47, 48). In those studies, it was observed that the concentration of the hydroxyl anions in the reaction mixture directly influenced the zeolite transformation rate, being the transformation of zeolite A into hydroxysodalite taking place indirectly through liquid phase without the formation of intermediate solid phases (see Figure 1) (47).

In a similar way, the same authors also studied the transformation of zeolite A into zeolite P in caustic media (47, 49). The kinetic study of this interzeolite transformation showed that

the zeolite A and zeolite P existed as discrete particles along the entire transformation process, suggesting the indirect transformation pathway through dissolution of starting material (49).

These mechanistic works on interzeolite transformations paved the way for the synthesis of new zeolites under OSDA-free conditions that otherwise would not be achieved using conventional synthesis (50, 51). Davis et al. used zeolite P as initial source to synthesize CIT-3 (HEU) (50) and CIT-4 (brewsterite) in presence of calcium and strontium cations, respectively. A dynamic equilibrium between the zeolite P and the dissolved species (aluminosilicates) was proposed, occurring the nucleation and crystal growth by condensation of the dissolved species (see Eq. 1) (50), similarly to the mechanism proposed by Subotic et al. (47).



2.1.2.- Mechanisms based on structural similarities between starting zeolite and product zeolite

Sano et al. have intensively studied the OSDA-free zeolite synthesis of zeolite through the interzeolite conversion method, mainly using FAU as initial source (52, 53). As it was also stated by other authors, Sano et al. observed that the presence of FAU as starting material increases the crystallization rate compared to conventional synthesis using amorphous aluminosilicates. The authors indicated that the enhanced crystallization rate could be attributed to the presence of small fragments (nanoparts) of ordered aluminosilicate species formed by the decomposition of the starting zeolite, and the assembling of these small fragments results in the crystallization of different zeolites (30). This mechanism has been clearly proposed for the transformation of LEV into CHA zeolite, since both structures contain the common SBU of *d6r* (double-six ring, see Figure 2) (31).

Other examples described by the same research group are the OSDA-free interzeolite transformation of FAU into Beta and MAZ zeolites (42). However, these structures do not share any common SBU, since FAU, Beta and MAZ present (*d6r, sod*), (*mor, bea, mtw*) and (*dsc, gme*), respectively (see Figure 2). Nevertheless, Sano et al. suggest that these samples still contain a common four-member ring (*4r*) chain, which is present within the *d6r, bea* and *gme* SBUs and, consequently, would serve as common building unit for their interzeolite

transformations. Similar explanations are described by Iglesia et al. for the OSDA-free interzeolite transformations of Beta into MFI and FAU into CHA, where the presence of common SBUs seems the main synthesis driving force, remarkably shortening the required crystallization times (32).

At this point, it is worth noting that the explanation of common SBU as intermediate during the transformation is based on the fact that the common SBU is present in both the starting and final materials. The direct characterization of the intermediates and establishing the kinetics of the synthesis on the bases of their available concentration in solution would be of great importance to achieve a deep mechanism understanding.

2.1.3.- Extended mechanisms to OSDA-free zeolite synthesis by seeding methods

It is well known since more than 50 years ago that the presence of a small amount of a particular zeolite acting as seeds in the synthesis media can not only increase the crystallization rates of this particular zeolite, but also can prevent the formation of undesired by-products (6, 54). However, the OSDA-free synthesis of zeolites by seeding methods has become relevant in the last ten years (41). Recently, much effort has been put into achieving an efficient preparation of the high-silica Beta zeolite without using an organic molecule as OSDA by the seeding method (55-58). It has been claimed that the initial Beta seeds are partially dissolved under hydrothermal conditions, allowing the growth of the new Beta crystals on the surface of the residual Beta seeds (59). Similar synthesis approaches using seeds with the same structure than targeted zeolites have been employed for the preparation of other OSDA-free zeolites, such as ZSM-12 (MTW) (60), ZSM-5 (MFI) (61), ferrierite (FER) (62), or RUB-13 (RTH) (63).

Interestingly, the OSDA-free synthesis of target zeolites using the seeding methodology can be extended to the use of seeds with different framework structures but containing common SBUs (41). An illustrative example is the synthesis of the high-silica ZSM-12 (MTW) using Beta zeolite seeds, where the ZSM-12 can be successfully synthesized from Beta seeds due to the presence of the common *mtw* unit (see Figure 3) (64).

2.2.- Mechanisms of interzeolite transformation using organocations

Beyond the OSDA-free synthesis routes described above, the particular combination of pre-crystallized zeolites and organic molecules as starting inorganic sources and OSDAs, respectively, has resulted in the efficient and selective preparation of many zeolite crystalline structures that could not be achieved using amorphous sources and/or OSDA-free conditions.

The first well-studied example on interzeolite transformations using organic molecules in zeolite synthesis was reported by Zones et al. using zeolite P as crystalline aluminosilicate precursor (65). This zeolite was always observed as intermediate during the synthesis of the high-silica Nu-3 zeolite (LEV) using N-methylquinuclidinium as OSDA (see Figure 4) (66). Through kinetic studies and high-resolution microscopy, the authors observed that the transformation of P to Nu-3 preferentially occurs contiguous to the zeolite P surface and not in solution, suggesting that the organocation would act as phase transport agent near the surface of the P zeolite (66). According to these early results, Zones et al. proposed that the solution/solid interface transportation could have an enormous importance in the nucleation and crystallization of zeolites when particular organocations are present in the synthesis media, resulting in the crystallization of different phases.

With the aim of getting better understanding of the interzeolite transformation mechanism, Sano et al. have systematically investigated the influence of several OSDAs on the hydrothermal conversion route (67-69). These systematic works suggest that during the interzeolite conversion process, the starting zeolite allows the formation of locally ordered aluminosilicate species (nanoparts) by decomposition/dissolution in the synthesis media, which would re-assemble and grow into different zeolite structures (see Figure 5) (30). These authors claim that the presence of these nanoparts permits rising the crystallization rate and improving the selectivity towards a particular zeolite (30).

2.3.- Interzeolite transformations from layered-preursors

If one expands the concept of building units from conventional SBUs with handful T atoms into a larger scale, it is reasonable to say that the layered substructures of certain three-dimensional frameworks are also one kind of building units. In fact, layer-containing frameworks are not rarely seen in zeolite structures. Structures like MWW, FER, CDO, AFO,

AST, MTF, RRO, RWR and SOD have been well-studied and some of them have already been put into important industrial processes (2, 13). Regarding the differences in crystallographic structures, the layered zeolites usually consist of stable layers connected by weak interactions or less stable SBUs. The differences in stability between layers and linkers render layered materials possibility to be manufactured through post-synthesis treatments. For this reason, the manipulation of layered zeolite or zeolite precursor is one of the promising strategy to obtain different zeolite structures (see Figure 6) (70).

The beginning of interlayer manipulation on layered materials could trace back to non-crystalline oxides, such as silicas, clays, and oxometallates (71). The principle strategy was intercalating organic compounds into the interlayer spaces to separate the layers, followed by insertion of more thermally stable inorganic compounds to serve as “pillar” and construct pillared layer structures (PLS) (72). The key to the success of this strategy is utilizing the different bonding strength of interlayer and intralayer parts of the structures.

Following the idea, the interlayer manipulation strategy should be applicable in zeolite materials with layered structures. For instance, in the case of MCM-22, the MWW layered precursor contains the OSDA molecules within the interlayer region, and the external surface of layers contains abundant silanol groups without linkage to adjacent layers. This layered material can either be pillared with organic silanes (71) or delaminated into single MWW layers through swelling/sonication treatments (73). These procedures were employed for other layered zeolite precursors, such as FER (74) and NSI (75-77).

Recently, this methodology has been extended to some germanosilicate zeolites (78). Ge atoms tend to occupy, at least partially, the crystallographic positions of some SBUs, such as the *d*4*r* units (21), being possible to create high-silica layers connected by germanium-containing *d*4*r* units within some particular germanosilicate frameworks (i.e. UTL) (79, 80). Since tetrahedrally coordinated Ge atoms are less stable and have high tendency to be extracted from the framework upon calcination or soft acid treatments (24), it is possible to take advantage of the chemical bond softness of Ge atoms to favor the crystallization of new zeolite structures following similar post-synthetic approaches to those reported previously (see Figure 6).

3.- Use of pre-crystallized zeolite precursors for optimizing the synthesis of target zeolites

3.1.- Synthesis of zeolite under OSDA-free conditions

Despite the extraordinary contribution of OSDA molecules in broadening the synthesis of new zeolite structures, introducing organic molecules always results in a remarkable increase of the costs associated with the zeolite preparation, and in some environmental issues related to the generation of harmful gaseous pollutants during the post-synthesis calcination (41). In order to alleviate these drawbacks, different approaches have been presented in the literature to efficiently conduct the synthesis of many industrially relevant zeolites in the absence of organic molecules, mainly based on the use of pre-crystallized zeolites as either full raw materials (42) or zeolite crystal seeds (41).

3.1.1.- OSDA-free synthesis of zeolites by interzeolite transformation

- *Synthesis of natural alkaline-earth zeolite analogues from a GIS-related precursor*

Davis et al. were one of the first researchers taking profit of the use of pre-crystallized zeolites to rationalize the synthesis of a series of natural alkaline-earth zeolites for the first time in the laboratory (81). The authors proposed the use of zeolite P1 (GIS) as starting material based on the fact that a GIS-related phase was the preferred intermediate crystalline phase achieved when they were studying the hydrothermal transformation of natural glasses (i.e. perlite) to zeolites in presence of aqueous calcium (82).

Thus, considering the use of a pre-crystallized zeolite P1 as initial source, the synthesis of the new CIT-3 (50) and CIT-4 (51) zeolites was described, presenting the heulandite (HEU, 8x10-ring pores) and brewsterite (BRE, 8x8-ring pores) structures, respectively. The authors combined the use of pre-crystallized zeolite P1 as aluminosilicate source with a calcium- or strontium-containing solution for the hydrothermal synthesis of CIT-3 and CIT-4 (see Figure 7a). Interestingly, the interzeolite transformation of the pre-crystallized GIS-related allows synthesizing the HEU and BRE materials in a pure form, precluding the presence of the impurities commonly found in natural zeolitic tuffs.

- *Synthesis of low-silica small pore zeolites by combining different alkali metal cations and FAU*

Martens et al. have recently described the efficient synthesis of four different Al-rich small pore zeolites following the interzeolite transformation of a low-silica FAU ($\text{Si}/\text{Al} = 2.6$) by studying the effect of different alkali metal hydroxides (83). Different zeolites were achieved after the hydrothermal treatments depending on the specific inorganic alkaline cation introduced in the synthesis media (see Figure 7b). In this sense, the resulting phases were ABW (8-ring), CHA (8x8x8-ring), MER (8x8x8-ring) and ANA (8x8x8-ring) when the $\text{NH}_4\text{-Y}$ zeolite was treated with Li, K, Rb, and Cs, respectively (83). This study clearly revealed that the presence of particular metal cations preferentially promotes the crystallization of specific zeolite frameworks.

To show the benefits of using the FAU zeolite as starting material, Martens et al. have studied the synthesis of the CHA zeolite employing other amorphous sources of silicon and aluminum under identical compositions, obtaining always amorphous materials (83). Thus, the authors conclude that the formation of other zeolites is significantly facilitated when an aluminosilicate source containing pre-existing connectivity is used, which will favor the crystallization of a particular zeolite even under much lower temperatures.

The catalytic properties of the OSDA-free CHA zeolite have been studied by Olsson et al. (84) and Davis et al. (85) for the selective catalytic reduction (SCR) of NO_x and methanol-to-olefins (MTO), respectively. Olsson et al. have reported that the fresh form of the Cu-exchanged low-silica CHA zeolite shows a good catalytic activity for the SCR of NO_x (84). Unfortunately, the relatively low Si/Al molar ratio together with the considerably presence of K^+ within the OSDA-free CHA zeolite, limit its high-temperature hydrothermal stability and, thus, its potential applicability. Therefore, it is demanded to increase the Si/Al molar ratio, either by direct synthesis or by post-synthetic treatments. In this way, Davis et al. have shown that some post-synthetic treatments, including steaming and acid wash, of the low-silica CHA ($\text{Si}/\text{Al} = 2.4$) favor the partial dealumination of the sample, creating an active and selective catalyst for the MTO process (85).

Finally, a very recent patent from researchers at Chevron describes the OSDA-free synthesis of the gmelinite (GME, 12x8x8-rings) by the hydrothermal conversion of FAU in presence of sodium cations (86). In this recent patent, it is claimed that the resulting GME zeolite presents a Si/Al molar ratio of ~ 2.5 , and the GME crystals are substantially free of non-GME

framework structures, such as CHA, which according to literature tend to intergrowth with GME (87). In addition, this material can be used for the selective separation of carbon dioxide (CO_2) from multi-component gas feedstreams.

- *Synthesis of high-silica zeolites from high-silica FAU and Beta zeolites*

Sano et al. have studied the use of high-silica FAU ($\text{Si}/\text{Al} \sim 8-22$) combined with seeds of the desired zeolite to synthesize different high-silica relevant zeolites by OSDA-free interzeolite transformations (52, 53). The OSDA-free high-silica Beta ($\text{Si}/\text{Al} \sim 11$) was achieved by combining the high-silica FAU and 9-20%wt of Beta seeds, together with NaOH in the synthesis media (53). Besides the OSDA-free Beta, Sano et al. have also described the synthesis of high-silica OSDA-free Levynite (LEV, 8x8-ring) (52) and OSDA-free Mazzite (MAZ, 12x8-ring) (88) by the hydrothermal conversion of high-silica FAU assisted by non-calcined crystals of LEV and MAZ as seeds, respectively. The resultant LEV and MAZ zeolites showed similar Si/Al molar ratios (~5.5-6.5), but the solid yields were relatively low (25-35%) (52, 88). The authors showed that the use of FAU as starting material resulted in a faster crystallization rate compared to conventional syntheses performed with amorphous aluminosilicate sources as initial raw materials. The favored formation of small ordered aluminosilicate species, nanoparts, through the decomposition/dissolution of the starting zeolite source in the synthesis media, allows enhancing the crystallization rate of the target zeolite, which in all the above cases show common SBUs with the starting zeolite (42).

According to the common composite building unit hypothesis, Sano et al. have also attempted the OSDA-free interzeolite transformation of Beta into ZSM-5 (MFI, 10x10-ring) (42). In this case, both Beta and ZSM-5 zeolites not only contain common 4- and 5-rings, but also the *mor* unit within their structures (see Figure 2). Due to the presence of these common units, the interzeolite transformation of Beta into ZSM-5 finished in merely two hours under the studied conditions, much faster than using traditional amorphous silicon and aluminum sources, where usually cost several days for a full crystallization. The resulting ZSM-5 zeolites synthesized through the interzeolite transformation procedure showed a Si/Al molar ratio of 15, but as occurred above with the samples synthesized from the high-silica FAU zeolites, the solid yield is low (below 20%).

In a similar way, Iglesia et al. have described the interzeolite transformation of high-silica FAU and Beta into high-silica ZSM-5 (see Table 1) (26). The authors have shown that the interzeolite transformation of high-silica FAU requires the presence of 10% of MFI seeds, whereas the interzeolite transformation of Beta could proceed in absence of seeds (see Table 1). These results clearly indicate that the nucleation and crystal growth become possible by the presence of common SBUs in both parent and target zeolites. The synthesis of other zeolites, such as CHA (8x8x8-ring), STF (10-ring) or MTW (12-ring), has been attempted by combining a high-silica FAU zeolite with the corresponding seeds of the target zeolites, but the resultant zeolites still presented a remarkable amount of amorphous phases.

In addition, Iglesia et al. have rationalized a process for encapsulating metal clusters within ZSM-5, taking advantage of its interzeolite transformation from Beta and FAU previously loaded with Pt, Ru or Rh (see Figure 8) (32). The metal clusters in the final metal-containing ZSM-5 zeolite show uniform sizes (\sim 1.3-1.7 nm), and their sufficient encapsulation have been determined by the relative hydrogenation rates of small (toluene) and large (alkyl arenes) molecules (32). This methodology can be a general strategy for the efficient encapsulation of metals within target zeolites.

3.1.2.- OSDA-free synthesis of zeolites by seeding methods

- *Synthesis of high-silica large pore Beta zeolite*

The OSDA-free synthesis of the high-silica Beta zeolite by the seed-assisted method has been intensively studied in recent years. The first synthesis description of the OSDA-free Beta zeolite was reported by Xiao et al. in 2008 (55). In this former work, the OSDA-Beta zeolite was prepared in its aluminosilicate form using a 10%wt of Beta seeds. The authors showed that the required crystallization time to obtain the OSDA-free Beta is very short (\sim 15 hours), comparable to the OSDA-guided Beta zeolite.

Following this work, other research groups have systematically studied the OSDA-free synthesis of Beta (56, 57, 59). Majano et al. studied the OSDA-free Beta synthesis under similar conditions to those reported by Xiao et al., but introducing different Si/Al molar ratios (Si/Al \sim 15-50), and using a Beta zeolite with a Si/Al ratio of \sim 26 as seed (56). However, the resultant Beta zeolite showed a relatively low Si/Al molar ratio (\sim 4), suggesting that this

material would present a limited hydrothermal stability. Thus, Okubo et al. studied the influence of other synthesis parameters in order to broaden the Si/Al ratio of the crystallized Beta zeolite (57, 59). By optimizing the composition of the synthesis gel, the Si/Al molar ratio of the resultant Beta zeolite increased up to 6.8, while presenting an excellent crystallinity. Moreover, the authors also reported the use of recycled OSDA-free Beta crystals as seeds, providing the crystallization of further generations of Beta without using OSDA, named “Green Beta synthesis” (see Figure 9).

The above-described OSDA-free Al-containing Beta zeolites have been tested as catalysts in different chemical processes. Yilmaz et al. have studied the catalytic activity of the OSDA-free Al-Beta zeolite for the alkylation of benzene with ethene and the hydroconversion of n-decane (89). The combination of large number of acid sites and large crystal sizes led to a fast catalyst deactivation by pore blocking for both reactions. However, an appropriate dealumination treatment allows not only delaying the catalyst deactivation but also improving the catalyst stability. In this sense, in benzene alkylation with ethene, the optimized OSDA-free Beta zeolite showed a higher selectivity toward the desired monoalkylated ethylbenzene product than commercial Beta zeolites, and in n-decane hydroconversion, the decrease of the amount of acid sites by dealumination resulted in higher isomerization yields than cracked products (89).

- Synthesis of other high-silica relevant large and medium-pore zeolites

Besides the synthesis of the OSDA-free Beta zeolite, other relevant large and medium-pore zeolites have been described in the last years by seeding methodology.

Okubo et al. have succeeded on the synthesis of the high-silica OSDA-free ZSM-12 zeolite (MTW, 12-ring) with Si/Al molar ratios ~11-16, by adding calcined ZSM-12 seed crystals (1-10%wt) (90). In contrast, the absence of ZSM-12 seeds favors the crystallization of other phases, such as MFI and/or MOR, indicating the crucial role of the MTW seeds. The authors also claimed the “Green MTW synthesis” by employing the OSDA-free MTW zeolite as seeds under consecutive OSDA-free MTW syntheses.

Valtchev et al. have reported the synthesis of the nanocrystalline ZSM-5 zeolite under OSDA-free conditions using silicalite-1 seeds (61). In this study, the authors have noticed that

the physico-chemical properties of the final product can be influenced not only by modifying the synthesis conditions, but also by altering the pretreatment of crystal seeds (i.e. drying and/or calcination). Under optimized synthesis conditions, the achieved nanocrystalline ZSM-5 materials showed an average crystal size of 30-70 nm and a Si/Al molar ratio of ~10 (61).

Okubo et al. have recently described the seed-directed synthesis of MWW-type zeolites from an OSDA-free Na-aluminosilicate gel (see Figure 10) (91). The authors claimed that, in this particular case, the MWW-seeds provided the surface for crystal growth and, for this reason, the use of as-synthesized MCM-22 seeds is required to prevent their complete dissolution in the synthesis media. The final solid yield of the achieved MWW material was ~40%, and the measured Si/Al molar ratio was ~11. The OSDA-free MWW zeolite has been tested for the Friedel-Crafts alkylation reaction of anisole with 1-phenylethanol, performing similarly than traditional MWW-zeolites.

- Synthesis of high-silica small pore zeolites

The synthesis of high-silica small pore zeolites under OSDA-free conditions has received a considerable attention in the last years, since it can be considered as a very attractive low-cost procedure to obtain efficient catalysts for some particular industrial processes, such as MTO or SCR of NO_x, among others (92).

From the recent high-silica OSDA-free small pore zeolites reported, the synthesis of high-silica TTZ-1 zeolite (RTH, 8x8-ring) is one of the most attractive descriptions, since this novel material is a good candidate for the selective production of propylene from methanol through the MTO process (63). The combination of sodium hydroxide with the use of calcined B-RUB-13 (RTH) crystals as seeds allowed the crystallization of the OSDA-free Al-containing TTZ-1 zeolite with Si/Al ~40. This material gave higher propylene selectivity (~44-47%) compared to other traditional small pore catalysts for the MTO reaction, such as SAPO-34 (~40-41%) (63).

Another interesting description via the seed-assisted OSDA-free method is the synthesis of Levyne (LEV, 8x8-ring) (58, 93). In this case, Xiao et al. have shown that the addition of a small amount of alcohols in the synthesis media favors the crystallization of the Al-containing

LEV, where the alcohol can be selected from methanol to n-butanol (93). The authors proposed that the presence of the alcohols would inhibit the crystallization of the undesired MOR zeolite. The resultant OSDA-free LEV material has good crystallinity, high surface area, uniform crystals, and a Si/Al molar ratio of ~4. This material had been tested for the MTO reaction and presented higher methanol conversion and selectivity towards ethylene (~42%) than other commercial MTO catalysts, such as ZSM-5 (~26%) or SAPO-34 (~31%) (93). However, limited hydrothermal stability caused by the low Si/Al molar ratio has to be considered.

The direct crystallization of CHA can also be prepared by a seed-assisted method in the absence of OSDA molecules, by combining the presence of K⁺ or Cs⁺ cations together with Na⁺ cations (94). The Si/Al molar ratio of the crystallized OSDA-free CHA can be increased to almost ~5 by the proper introduction of Cs⁺ in the initial synthesis gel replacing part of the K⁺. In addition, the effect of boron in the initial gel has been studied, since the presence of B³⁺ instead of Al³⁺ in the CHA framework could lead to a CHA zeolite with a higher Si/Al molar ratio. Following the boron strategy, Tatsumi et al. have synthesized a CHA zeolite with a final Si/Al molar ratio of 6.1 (94). These OSDA-free CHA materials have been also tested for the MTO reaction, and some of these materials approach the catalytic behavior of the commercial Al-SSZ-13 catalyst, both in terms of catalyst lifetime (140-150 min) and olefin selectivity (~30% and ~35% for C2⁼ and C3⁼, respectively) (94).

3.2.- Synthesis of zeolite through interzeolite transformation assisted by organotemplates

The early descriptions combining the use of zeolite phase transformation with an organotemplate employed FAU-related materials and tetramethylammonium (TMA) cations for the synthesis of the large pore ZSM-4 zeolite (Omega, 12x8-rings) (95, 96). These former syntheses paved the way for the preparation of many crystalline structures combining a pre-crystallized zeolite and an organotemplate molecule. Some of the most relevant descriptions are summarized below attending to their pore topology.

3.2.1.- Synthesis of small pore zeolite via interzeolite transformation

- High-silica CHA zeolite

The synthesis of chabazite (CHA, 8x8x8-rings) from amorphous sources was reported by Zones using *N,N,N*-trimethyladamantammonium (TMAda, see Figure 11) as template (97). The author noticed the formation of an intermediate crystalline phase, zeolite P, during the CHA synthesis (98). Then, according to this discovery and as proof of concept, Zones proposed the use of the cubic P zeolite as silicate precursor and realized the interzeolite conversion to CHA (65). Soon after this work, the phase transformation from FAU to CHA was also reported by Zones, where it was observed that the combination of the FAU source together with the TMAda cation allows increasing not only the crystallization rates towards the CHA zeolite, but also their final Si/Al molar ratios (33).

Due to the high industrial value of CHA-related zeolites, its synthesis following the interzeolite transformation has been extensively investigated in the last years. Sano et al. described that the transformation of FAU to CHA using benzyltrimethylammonium (BzTMA, see Figure 11), allowing the substitution of the expensive TMAda template (99). This procedure results in the crystallization of a high-silica CHA material with a Si/Al ratio of 16. Further adding crystals of CHA into the synthesis gel as seeds permit broadening the Si/Al (13.4-21.5) and shortening crystallization time (35). Moreover, the CHA obtained through this method showed higher resistance against acid-treatments than the conventional SSZ-13 (100), providing excellent separation capabilities for feeds containing mixtures of water and acetic acid (see Figure 12) (101). Moreover, Sano et al. have described that adjusting the Si/Al of the starting FAU in combination with BzTMA as OSDA allows reducing the crystal sizes of the resultant CHA to the nanometer scale (~ 100 nm), preferentially when the Si/Al ratios of the initial FAU were fixed between 35-60 (102). The nanosized CHA zeolite performed with high catalytic activity for the ethanol to propylene reaction (102).

Very recently, Corma et al. have reported the efficient synthesis of the high-silica CHA zeolite using tetraethylammonium (TEA, see Figure 11), a less-expensive OSDA than those previously employed in the literature, and pre-crystallized FAU zeolites as the sole silicon and aluminum source (see Figure 13) (27). The authors proposed that the particular presence of common *d6r* SBUs in the former FAU zeolite would be the main driving force of the formation of the CHA zeolite when using TEA as OSDA, since the use of other amorphous or crystalline zeolites as initial silicon and aluminum sources mostly results in the crystallization

of Beta zeolite (27). Very interestingly, they showed the incorporation of Cu and Fe species within the resultant high-silica CHA zeolite, both by post-synthetic cation exchange or by a one-pot synthesis procedure, allowing the preparation of catalysts with an excellent NH₃-SCR of NOx activity (27, 103).

Xiao et al. have further optimized the synthesis conditions of interzeolite transformation from FAU to CHA into a solvent-free system using *N,N,N*-dimethylethylcyclohexylammonium (DMECHA, see Figure 11) as OSDA (104). In this description, water was not added as solvent during the gel preparation, remaining the mixture as solid throughout the entire synthesis procedure. The authors claimed that the absence of water as solvent enhanced solid yield of synthesis by avoiding dissolution of framework aluminosilicate species. The addition of crystal seeds was required to guarantee the crystallization of the high-silica CHA zeolite (104). When exchanged with Cu, this solvent-free CHA zeolite showed similar NO conversion values than well-known Cu-SSZ-13 catalysts prepared by regular hydrothermal routes for the NH₃-SCR of NOx.

Finally, Sano et al. have shown that the incorporation of different heterometal atoms (M) within an aluminum-containing high-silica FAU zeolite could also lead to the formation of [Al, M]-CHA by the corresponding interzeolite transformation synthesis (105, 106). Up to now, there is no record of the synthesis of [Al, M]-CHA materials from amorphous hydrogels. When the synthesis started with FAU zeolites containing different metals, such as Fe, Ga, Ti, Sn, bimetallic CHA zeolites were synthesized following this rationalized interzeolite conversion method using TMAda as OSDA. The catalytic behavior of these bimetallic CHA zeolites has been tested for the NH₃-SCR of NOx after introducing Cu cations by post-synthetic cation exchange. Noticeably, the Cu-containing [Al, Sn]-CHA catalyst shows higher hydrothermal stability than regular Cu-CHA, even after hydrothermal treatments at 900°C.

- Other clathrasils and high-silica small pore zeolites

Despite the fact that clathrasils, a family of zeolite-type structures containing only 6-T atoms as largest rings, can hardly be specifically considered as small-pore zeolites, Sano et al. recently described the synthesis of two clathrates following the interzeolite transformation

of FAU using organotemplates. On one hand, the RUB-10 (RUT) zeolite has been synthesized combining high-silica FAU zeolites together with tetramethylammonium hydroxide (69), where the presence of FAU as starting material clearly increased the crystallization rate. On the other hand, the co-existence of benzyltrimethylammonium (BzTMA) and sodium chloride was able to direct the FAU conversion to ZSM-39 (MTN) zeolite (107). No sign of BzTMA was observed in the resultant MTN zeolite while the presence of tetramethylammonium and trimethylamine was suggested, indicating a decomposition of BzTMA during the synthesis.

Besides CHA, other high-silica small pore zeolites have been described. Sano et al. reported the conversion of FAU into LEV (8x8-rings) in the presence of choline hydroxide under whose conditions no crystalline phase was observed from amorphous aluminosilicate gels, undoubtedly proving the advantage of the use of the crystalline aluminosilicate precursor (34). The resultant LEV zeolites showed high Si/Al molar ratios (~9-12), and they performed as excellent catalysts for the conversion of ethanol to light olefins (ETO), with high yields to ethylene and propylene (~36 and 34, respectively). The same authors also reported the conversion of FAU to LEV in fluoride media using 1-adamantanamine as OSDA (108). In this case, the Si/Al molar ratios of the achieved LEV materials were higher than those obtained previously through the interzeolite transformation in alkaline conditions (Si/Al~13-29). It was suggested that during the same morphological transformation, in this case FAU to LEV, hydroxide and fluoride media gave different decomposition/dissolution rate. That is, the dissolution of parent FAU would be slower in fluoride media than in hydroxide media and, as a consequence, the nucleation as well as crystallization would take place before parent FAU was completely consumed in fluoride media (108). More recently, researchers at Chevron have described a similar synthesis methodology for achieving the LEV-type zeolite from FAU in fluoride media using an alternative OSDA, i.e. N-methyl quinuclidinium (109).

The aluminosilicate form of the AEI structure, SSZ-39, is another important small pore zeolite that, in the last years, has received significant attention for its great potential applicability in DeNOx and methanol conversion reactions (110, 111). This material was first described by Zones et al. using different alkyl-substituted cyclic ammonium cations and sodium silicates as OSDAs and amorphous sources of silicon, respectively (112, 113). Unfortunately, this former synthesis recipe results in crystalline SSZ-39 materials with low solid yields (below 50%),

limiting the potential use of this zeolite in commercial applications. In an attempt to increase the efficiency of the SSZ-39 synthesis, two different research groups have independently proposed the interzeolite transformation procedure starting from high-silica FAU materials using different OSDA molecules (28, 36). On one hand, Sano et al. proposed the use of tetraethylphosphonium (TEP, see Figure 14) as OSDA in combination with different high-silica FAU zeolites, allowing the preparation of crystalline SSZ-39 zeolites with Si/Al molar ratios (~13-20), and solid yields above 80% (28). On the other hand, Corma et al. have also described the zeolite-to-zeolite transformation procedure for the preparation of the high-silica SSZ-39 material combining a high-silica FAU zeolite with *N,N*-dimethyl-3,5-dimethylpiperidinium (DMP, see Figure 14) as OSDA, resulting in crystalline SSZ-39 materials with Si/Al molar ratios between 8-10 and solid yields above 80% (36). More recently, other authors have also reported similar interzeolite FAU-AEI transformations using DMP or related-OSDA molecules (i.e. *N,N*-diethyl-2,6-dimethylpiperidinium, DEDMP, see Figure 14) (114, 115).

The Cu-species had been introduced into the above described SSZ-39 materials through either post-synthetic cation exchange procedures (28, 36) or, in the particular case of the AEI-type catalyst prepared using DMP, one-pot synthesis methods (36). The resultant Cu-SSZ-39 catalysts showed excellent catalytic activity for the SCR of NO_x reaction and the phosphorous-free Cu-SSZ-39 catalysts presented a substantially higher hydrothermal stability when aged under harsh conditions (i.e. steaming at 750°C) (36). Interestingly, Corma et al. also succeeded in preparing the iron-containing SSZ-39 under similar interzeolite transformation methodology using DMP as OSDA, either by post-treatment ion-exchange or one-pot transformation introducing iron nitrate in the synthesis gel (116). Particularly, the one-pot prepared Fe-based SSZ-39 showed better hydrothermal stability and catalytic activity compared to other related Fe-containing zeolites for the high-temperature NH₃-SCR of NO_x, which could be assigned to better dispersion of Fe species (116).

By adjusting the synthesis conditions reported by Sano et al. for the interzeolite transformation of FAU into SSZ-39 using tetraethylphosphonium (TEP) as OSDA (28), Corma et al. recently described the preparation of the SSZ-39 material in its nanocrystalline form (~50-60 nm) (117). The authors suggested that the use of FAU as zeolitic precursor under the

adequate synthesis conditions could favor the formation of AEI-precursor nuclei thanks to the presence of common SBUs in both materials, increasing the nucleation and crystallization rates. The nanosized SSZ-39 has been tested as catalyst for the MTO reaction, obtaining remarkably longer catalyst lifetimes compared to conventional CHA and AEI-related materials (117).

Finally, Martin et al. have shown the interzeolite transformation synthesis of two zeolites with large cavity sizes, ERI and AFX, using a bulky polycyclic template (see Figure 15) (118).

The sizes of the bulky polycyclic template ($11.9 \times 4.9 \text{ \AA}$) fitted perfectly with that of the very large cavities ($\sim 13 \text{ \AA}$), proving an excellent structure-directing role towards ERI and AFX cavities. The introduction of copper and iron cationic species within these ERI and AFX, results in very active SCR-NO_x catalysts with similar NO conversion profiles to well-established commercial metal-containing SSZ-13 catalysts.

3.2.2.- Synthesis of medium and large pore zeolite via interzeolite transformation

Different zeolites with 10- or 12-rings have also been reported in the literature following interzeolite transformation procedures. Some of the most relevant descriptions are here summarized.

Sano et al. realized transformation from dealuminated FAU to Beta ($12 \times 12 \times 12$ -rings) in assistance with tetraethylammonium hydroxide (TEAOH) (67). Although Beta can also be obtained using amorphous silicon and aluminum source, the crystallization rate was faster in the case of FAU conversion (67). The same group later reported that using BzTMA together with Li⁺ and Na⁺ could lead to formation of OFF zeolite (12×8 -rings), which otherwise cannot be obtained from amorphous sources (119).

Kubota et al. reported the transformation from FAU to MCM-68 zeolite (MSE, $12 \times 10 \times 10$ -rings), using a dipyrrolidinium template (37). The authors described that the locally ordered aluminosilicate species resulting from the decomposition of the former FAU-type source, increase the nucleation and crystallization rates, shortening the former crystallization period of 16 days to only 3 days. (34, 120). Zhang et al. also proposed the transformation from FAU to MWW (121), thanks to a synergistic effect between the organic template

hexamethyleneimine (HMI), NaOH, and SiO₂ (121). This MWW was tested in liquid-phase alkylation of benzene with ethylene and showed improvement in ethylene conversion and ethylbenzene selectivity, probably due to its lower crystal size (121). Davis et al. reported a successful synthesis of IWV (ITQ-27, 12x12-rings) zeolite from FAU using tetramethylimidazole-based diquats with varying linker lengths as template (122). In its original report, ITQ-27 was synthesized using dimethyldiphenylphosphonium as template under hydrothermal condition for 59 days (19). The transformation from FAU rendered facile synthesis using easily synthesized template and obviously shortened the crystallization time. Zeolites other than FAU have also been adopted as starting material for interzeolite transformations. Starting with boron-containing beta zeolite, using several different organic templates, Zones et al. achieved transformations into SSZ-24 (AFI) and SSZ-31 (*STO), both possessing 12-rings in their structures (123). The results indicate that the transformation was not simply a rearrangement of beta but a dissolution/reconstruction process. The relatively fragile B-O-Si bond broke during synthesis and reassembled into other phases in assistance of templates (123). Later, the aluminosilicate forms of SSZ-24 and SSZ-31 were synthesized by Sugi et al. also through transformation from Al-BEA (124, 125). It has been speculated that the apparent phase transformation from Al-BEA to Al-SSZ-24 is initiated by the dissolution of Beta to some minimum four-ring structural units followed by its redirection towards SSZ-24 phase in the presence of the OSDA (126). The catalytic performance of Al-SSZ-24 synthesized by direct transformation from Al-BEA was compared with Al isomorphous substituted B-SSZ-24 in the isopropylation of biphenyl. The Al-SSZ-24 from interzeolite transformation showed better shape selectivity towards the desired 4,4'-diisopropylbiphenyl isomer (126). The authors proposed that the other non-selective alkylated isomer products would mainly be formed in the aluminum species present on the external surface of the crystals, indicating that the direct transformation of the Al-Beta favors the aluminum distribution along the entire SSZ-24 crystals (126).

3.2.3.- Synthesis of mesoporous zeolites via interzeolite transformation

Inspired by the discovery of the MCM-related mesoporous materials, a series of materials containing pore openings above 20 Å (127, 128), many researchers have devoted themselves

to develop new synthesis approaches and applications for these amorphous materials with ultra-large pores (129). However, these mesoporous materials show low hydrothermal stability and acidity, severely limiting their applicability in many industrial catalytic processes. Thus, in order to overcome these problems, the efficient preparation of mesoporous zeolites, which would present at meantime high hydrothermal stability, acidity and pore accessibility thanks to the crystalline frameworks combined with the presence of the mesopores, has been deeply investigated in the last years (130, 131). One of the preferred synthesis routes to generate the mesoporosity within the crystalline zeolites is based on the post-synthetic dealumination and/or desilication with an acid or a base, creating the mesopores by extracting atoms from the zeolite framework (130). However, this method could present two important drawbacks. One is the non-homogenous mesoporosity along the zeolitic crystals, and the other is the low atom-efficiency due to the leaching of the framework atoms during the post-synthetic treatments. In this sense, other surfactant-based constructive methods have been described employing different silicon and aluminum sources to overcome these problems (131). In particular, Gérardin et al. (132) and García-Martínez et al. (133) have recently described the pseudomorphic transformation of a parent high-silica FAU zeolite (USY) into a mesoporous zeolite Y by recrystallization in the presence of surfactants in the synthesis media (see Figure 16). These mesostructured USY zeolites showed high-crystallinity, acidity and hydrothermal stability, with improved gasoline and diesel selectivities for the fluid catalytic cracking (FCC) process when compared to classical FAU catalysts (133). A similar methodology was described by Xiao et al. for the synthesis of low silica mesoporous Na-X zeolite (FAU structure) combining the use of a precrystallized Na-X precursor using a cationic polymer (polydiallyldimethylammonium chloride) (134).

3.3.- Synthesis of zeolite through interzeolite transformation from layered precursor

Interlayer expansion or condensation of preformed zeolitic layered precursors enable their transformation into delaminated two-dimensional or new three-dimensional zeolite structures, respectively (135). Indeed, the delicate selection of the post-synthetic treatments on the former layered zeolitic materials, could allow controlling the final crystalline structure (i.e. pore topology) or the physico-chemical properties (i.e external surface area or

heteroatom introduction) of the resultant zeolite (135, 136). Besides traditional high-silica layered structures, Morris et al. have recently extended this concept to germanosilicate zeolites through the so-called ADOR (assembly-disassembly-organization-reassembly) methodology (78). Hereby, the most relevant achievements for the topotactic transformation or delamination of preformed zeolite-based layered precursors are summarized.

3.3.1.- MWW family zeolites

One of the milestones in the field of layered zeolite is the successful synthesis of MCM-22 family zeolite in 1994 by Mobil (137). In the as-synthesized form of MCM-22, the MCM-22P, the monolayers are not connected and interlayer spaces are filled by bulky organic templates (see Figure 17). Inside the layer is a set of bidimensional 10-ring channel system and, more interestingly, a hexagonal array of 12-ring “cups” that penetrate into the sheet from both sides. If the precursor is calcined directly after synthesis, the template will be eliminated and the MWW layers will condense through dehydration of silanol groups, forming three-dimensional MWW zeolite (MCM-22), with two independent multidimensional channel system and a unique supercage (see Figure 17). If carefully adjust the molar ratio of organic template and inorganic cations, the three-dimensional framework of MWW, instead of separated as layered precursor by OSDA layer, can be directly synthesized, named MCM-49 (138).

In principle, the manipulations of MCM-22P start with intercalation of the material with large organic molecules, also known as swelling, to expand the interlayer space. The first attempt in swelling of MCM-22P was carried out by Roth et al. mimicking precedent treatments to other layered materials such as silicas, clays or metal oxides. An interlayer pillaring using organosilane solutions easily produced the new layered material MCM-36 (71). The material maintained the unique structural characteristics of MCM-22 monolayer while the interlayer space being expanded (see Figure 17). Instead of using silicon species as pillar, Corma et al. conducted pillaring of MCM-22P using organic silyl-arylic groups as linkers and obtained an organic-inorganic hybrid multilayer bifunctional MCM-22 derivative, named MWW-BTEB (139).

Starting from swelled MCM-22P, Corma et al. succeeded in preparing delaminated MCM-22,

named ITQ-2 (73). After being swelled with surfactant, the MCM-22P were forced apart with ultrasound bath or by vigorous stirring, and the collected solid contains a structure with single layer of MWW, exposing the 12-ring cups while preserving the circular 10-ring microporous system (see Figure 17). The well-defined external surface area together with larger number of cups in ITQ-2 give the material a larger amount of structurally accessible acid sites which results in superior catalytic activity in a large number of reactions (140).

Other novel crystalline structures can also be obtained starting from MWW-related precursors. Recently, Wu et al. reported that through a dissolution-recrystallization route (RDR), the pure silica 3D MWW zeolite (141), can direct a novel intergrowth of MWW monolayers, resulting in two new different polymorphs, ECNU-5A and ECNU-5B (see Figure 18) (142). Through the RDR treatment, the sinusoidal 10-ring channel was well-preserved while the interlayer channel system were transformed into zigzag shape. The geometry mismatch between OSDA, 1,3-bis(cyclohexyl) imidazolium, and zeolite framework is ascribed to be the reason for such zeolite layer shift. On the other hand, Fan et al. reported an interlayer expanded Ti-incorporated MWW analogue zeolite, Ti-YNU-1, when subjecting Ti-containing MWW precursors to a high temperature acid treatment (39). It is suggested that the interlayer expansion was a result of the intercalation of monomeric Si species leached during the treatment.

The versatile structural transformations render MWW family structure possibilities in modification for various applications. In a series of research, Corma et al. proved that in cracking of larger feedstocks, such as di-isopropylbenzene and vacuum gasoil, ITQ-2 with delaminated structure, compared to three-dimensional MWW-type zeolite, is more active and selective to valuable gasoline and diesel products and less low-value gas and coke (73, 140, 143). Moreover, the selectivity and deactivation of ITQ-2 catalyst in alkylaromatic catalytic transformations could be tuned by different degree of delamination (144).

Modified MWW-zeolites behave utterly not only in cracking of large feedstocks, but also in fine chemical productions, especially those with bulk reactants (145, 146). By grafting titanocene on ITQ-2 material, Corma et al. succeeded in preparing Ti-containing ITQ-2 as a catalyst for epoxidation of alkene. The material showed high conversion of bulky substrate cyclohexene together with high target epoxide (147).

The potential of layered zeolites manipulation are not limited in the area as acid catalysis. Corma et al. mixed a stabilized platinum-DMF solution with the swelling mixture of ITQ-1 and controlled the treating temperature. The Pt particles in the resultant Pt-MWW have average particle sizes of less than 0.7 nm and, more interestingly, are encapsulated in the interlayer cavities of MWW during the calcination (see Figure 19) (148). The activity of such catalyst is nearly six times higher than normal Pt loaded by impregnation and could remain against frequent reaction-regeneration cycles at high temperature. The small cluster size, high activity and stability is due to the spatial confinement of MWW framework as a result of layer engineering.

The facile and versatile manipulation of MCM-22 family zeolites, both from direct synthesis or post-synthesis modifications, has proven the high potential of engineering layered zeolites and their application in industrial processes.

3.3.2.- Other layered precursors

The pioneer works in interlayer engineering of MWW type layer zeolites showed an excellent example of enormous possibilities in structural engineering of layered zeolite precursors.

Another 3D zeolite composed of linked layer substructure that has been well studied is ferrierite (FER). Ferrierite was first discovered as a natural mineral and later has been characterized to have lamellar crystal framework structure (149). In FER obtained from traditional synthesis, the framework is connected in three dimension directly (150). With assistance of a bulky template in fluoride synthesis media, Caullet et al. obtained for the first time a preserved FER structure with larger interlayer distance, named PREFER (see Figure 20) (151). Other syntheses of PREFER have also been reported from the non-amorphous precursor H-kanemite in assistance of tetramethylammonium, named PLS-3 (152, 153), or using specific di-quaternary ammonium salts as OSDAs (154). Another PREFER material, named ITQ-19, was synthesized by Corma et al. using 1,4-diazabicyclo[2.2.2]octane as OSDA (155). This synthesis enables introducing high amounts of tetrahedral coordinated aluminum in the final material.

Delamination of PREFER into single FER layers, ITQ-6, has been soon realized by Corma et al. through swelling of PREFER with assistance of cetyltrimethylammonium bromide and

tetrapropylammonium hydroxide (see Figure 20) (74). The peak shift along treatment illustrated the process of expansion and exfoliation. Meanwhile, the BET area of ITQ-6 has three-fold increased (74), being the delamination level tuned by different treatments (156).

The arrangement between FER monolayers could be different, and produce another related structure, named CDO (see Figure 21-right) (157). The CDO structure has been reported in different layered silicates materials such as MCM-65, PLS-1, PLS-4 and HUS-4 (158-160). Analogous to the case of PREFER, pillaring and interlayer expansion treatment has also succeeded in the case of CDO lamellar structures (161, 162).

Zeolite NSI, another zeolite framework composed of layered substructure, was first obtained via an indirect layered precursor named Nu-6(1) using as OSDA 4,4'-dipyridine in 1983 (163). Nevertheless, its crystalline structure was not recognized until twenty years later, which is formed by 5-rings connected by sharing edges, similarly to FER and CDO but different in spatial symmetry (164). After calcination to remove organic template in Nu-6(1), a three-dimensional small-pore framework material, Nu-6(2), was obtained through interlayer condensation (164). Swelling the precursor Nu-6(1) with decyltrimethylammonium (DTMA), a full delamination was observed, resulting in the delaminated ITQ-18 zeolite (75). Pillaring the layered Nu-6(1) precursor with an organosilane, Roth et al. obtained the pillared material with NSI monolayer, named MCM-39 (76, 77). Being topologic analogue to NSI structure, zeolite CAS is known to be composed of CAS layers stacked in the NSI configuration. Such material was named EU-19 while, different with Nu-6(1), Nu-6(2) was not obtained when treated upon calcination (165). Instead, the resultant material, EU-20, has an unidentified structure (166). The isomorphic structure observed between Nu-6(1) and EU-19 shows a good example of how the interlayer manipulation could be influenced by even subtle mismatch between layers.

3.3.3.- Germanium-containing layered zeolites

It was shown in 2002 that introducing germanium in zeolite synthesis was an effective way to generate synthesis gels that include abundant double four-member rings (*d4r*), leading to formation of zeolites with special *d4r* building blocks (21). In these Ge-containing zeolite, the location of germanium is not random and is preferentially located as member of the *d4r* (21).

Moreover, it was postulated that introducing $d4r$ in the structure should lead to extra-large pore zeolites (22-24, 167).

Among all those zeolites obtained through Ge-assisted synthesis, ITQ-15 with topotactic structure code UTL is appealing due to its unique framework structure, since it possesses a 14×12 -ring channel system (22, 168). Germanium in UTL is preferentially located in the $d4r$ interlayer, generating different stability between the dense ferrierite-type layers and interlayer parts (see Figure 22). Upon acid hydrolysis, the less stable $d4r$ could decompose, leading to a partially degradation of 3D UTL framework into separated 2D dense layers (169). Based on the unique structural feature of UTL zeolite, Martens et al. (80) and Morris et al. (79) developed a method to transform a previously assembled zeolite into new zeolite structures through a combination of destructive and constructive methods, named ADOR process (79, 80). The ADOR process is generally divided into the following distinguished steps:

- (i) The first step is the assembly, where the pre-crystallized zeolite precursor is firstly obtained through hydrothermal synthesis. The most studied zeolite precursor is IPC-1P, analogous to ITQ-15 and IM-12, with UTL structure. The Si/Ge ratio in the as-synthesized IPC-1P could vary (~4.3-6.0), equal to the chemical composition in the range of $d4r$ [7Ge, 1Si] to [5Ge, 3Si] (170). The presence of Ge-rich $d4r$ in layered zeolites is not exclusive in UTL structure. In fact, zeolites such as ITQ-22 (IWW) (171), ITQ-24 (IWR) (172), or ITQ-13 (ITH) (173) were also reported to have similar layered structures connected by Ge-rich $d4r$ units.
- (ii) The second step of ADOR process is the disassembly of the abovementioned pre-crystallized zeolite precursor. The instability of Ge-containing zeolites, usually seen as a crucial disadvantage of such materials, is here utilized to modify the Ge-containing zeolite precursor. Through a calcination in air followed with acid treatment, an obvious change in the PXRD pattern of the material could be observed, indicating a partial degradation of the parent UTL zeolite (169). When starting UTL material contains proper amount of germanium, the layer could disconnected from each other, resulting in a unilamellar material, IPC-1P (169). IPC-1P possesses *utl* layers with thickness of approximately 9 Å and Si/Ge ratio of ~26-37, significantly higher than the parent UTL material. Systematical studies have revealed that multiple factors, such as acid concentration, treating temperature and/or Ge content in

parent zeolite, are influencing the hydrolysis process and could lead to different outcome product (78). Different with in the case of MCM-22P and PREFER, the disassembled IPC-1P is not a well stacked layer material. Upon calcination, the obtained IPC-1 is a poorly ordered sub-zeolite, which is thought to have a partially collapsed structure (169).

(iii) The disassembly of UTL into layered IPC-1P generates countless possibilities in its structural engineering. The following ADOR step is the so-called organization/reassembly step. In fact, the organization is not always separated from the disassembly step. When 3D UTL zeolite is treated with acid solution, two controversial processes is going at the same time, the de-intercalation of framework Si atoms and the reorganization of framework Si atoms to form new bonds (78, 79). Upon calcination, such de-intercalated material forms a 3D material, IPC-4, with 10x8-ring channels. Along with acidity of treating solution increases, another mechanism occurs. Starting from the germanosilicate with UTL structure, Kirschhock et al. previously reported an inverse sigma transformation process during which germanium four-rings (*Ge4r*) were washed and shifted into zeolite channels while the positions of previous *d4r* were replaced by silicon four-rings (*Si4r*) (80). The resultant material, named COK-14, possesses 12x10-ring channel system as a result of pore expansion by *Si4r* units between layers. In a similar way, Morris et al. later achieved the IPC-2 material, which is isostructural to COK-14 (79). Both IPC-2 (or COK-14) and IPC-4 possess the dense layer inherited from IPC-1P, being the layers of IPC-2 connected by single four-member ring (*s4r*) and those of IPC-4 through silanol condensations (see Figure 22). The occurrence of *s4r* is the result of rearrangement of framework Si caused by high acidity.

Other than the acid treatment, the presence of an organization agent could generate possibilities of the structure variation. Once the layers have been separated by exfoliation, the interlayer manipulations described previously in the cases of MWW and FER families are possible to be applied (169, 174).

Beyond UTL-based germanosilicates, Morris and Cejka et al. have expanded the ADOR methodology to the use of other germanosilicate layered-based materials, such as ITQ-22 (IWW, 12x10x8-rings) (175), IM-17 (UOV, 12x10x8-rings) (176), and CIT-5 (CFI, 14-rings) (177), as former crystalline precursors to achieve the synthesis of new zeolite frameworks, including IPC-12 (12x8-rings), IPC-15 (10-rings), and IPC-16 (12-rings) (see Figure 23) (177).

4.- Perspectives

Along the present review, it has been shown the unique inorganic directing roles provided by the use of pre-crystallized zeolite-based sources, permitting not only the synthesis of novel zeolite frameworks but also the improvement of the physico-chemical properties of many known zeolitic structures that otherwise would not be obtained using more traditional amorphous sources. Following diverse interzeolite transformation strategies, it has been possible to synthesize nanosized zeolites, inexpensive OSDA-free industrially-relevant zeolites or selectively introduce heteroatoms to design very active metal-containing zeolites, among others. All these advances have introduced new fundamental knowledge and questions in the field, which would allow the rationalization of future synthesis procedures to efficiently direct the crystallization of target zeolite frameworks with the desired physico-chemical properties.

Many zeolites with different pore topologies have been described under OSDA-free conditions using the seeding or the interzeolite transformation methodologies. In fact, the OSDA-free syntheses of industrially-relevant zeolites ranging from small-pores (i.e. CHA) (94) to large-pore zeolites (i.e Beta) (89) have been described in the literature. Although the undoubtedly advances that these synthesis protocols offer for their potential industrial implementation, future work must focus on increasing the chemical composition window (i.e. higher Si/Al molar ratios) and the solid yields obtained through the OSDA-free methods (usually lower than 50%). We can speculate that the use of pre-crystallized zeolites as initial sources, combined with particular synthesis conditions (lower H₂O/Si ratios and low-moderate pHs) may increase chemical window compositions and/or solid yields.

In this sense, the introduction of inexpensive amine or ammonium molecules in the synthesis media has been demonstrated that can act as organic pore fillers, permitting the partial or total substitution of the alkali or alkaline-earth cations, and resulting in zeolites with remarkably higher Si/Al molar ratios and solid yields (27, 178). This methodology can be extended to other catalytically attractive zeolites, which currently require the use of expensive and sophisticated OSDA molecules.

The preparation of hierarchical zeolites containing well-defined mesoporosity is an

outstanding challenge in catalysis, since these mesoporous zeolites can improve the molecular diffusion pathways while maintaining the hydrothermal stability compared to classical microporous zeolites. The recent use of a pre-crystallized zeolite as silicon source (i.e. FAU) combined with a long-chain amphiphilic surfactant as supramolecular template to generate the mesopores within the zeolite crystals, has allowed the preparation of high-silica mesoporous-containing FAU zeolites with excellent properties to act as highly-stable catalyst for chemical processes involving bulky molecules (132, 133). This surfactant-based interzeolite transformation methodology could be extended to the preparation of other hierarchical zeolites with application in very diverse chemical processes. Nevertheless, it would be of interest to reduce the costs associated to the use of the long-chain amphiphilic surfactant and, in this sense, we propose its partial or total substitution by other organic molecules with shorter alkyl chains (i.e. below C6).

Another very challenging approach in catalysis is the design of metal-containing zeolites presenting exceptional control on the nature of the metal species, mainly metallic clusters or small nanoparticles, making special emphasis on maximizing the metal confinement within the pores and cavities of zeolites, with the aim of increasing shape-selectivity and metal stability (179-182). Considering this, the recent descriptions of Iglesia et al. (32) and Corma et al. (148) introducing the required metal species within preformed zeolite precursors open new frontiers in the design of metal-confined catalysts, even for the efficient preparation of bimetallic-based novel heterogeneous catalysts.

The preparation of 2-D zeolite layered materials has allowed their implementation in many diverse chemical processes, from petrochemistry to fine chemistry and biomass transformations involving bulky organic molecules (73, 74, 143, 146, 147). Current exciting trends would embrace the fine-tuning control of the layered thickness avoiding the multistep synthesis procedure or the use of expensive organic surfactants. In this sense, the simple cyclic ammonium cations with short alkyl chains (C₃ to C₆) that have been recently employed for the synthesis of different nanozeolites (183-185), could be used to attempt the surfactant-free preparation of zeolitic-layered materials with thickness in the nanometer scale. A plausible synthesis strategy could combine these simple organic molecules with seeds of the desired layered zeolite in the synthesis media.

The introduction of germanium allowed the synthesis of many extra-large pore germanosilicates, in where was demonstrated that Ge atoms preferentially occupies the *d4r* units (21). This fact allowed the recently described post-synthetic transformation of the germanosilicate materials containing high-silica layers connected through *d4r* units into new high-silica zeolite structures (78). This methodology, so-called ADOR, is a rationalized approach to control the pore topology of novel zeolite frameworks, from small pore to extra-large pore zeolites. However, and despite the large versatility in designing novel crystallographic frameworks, the inclusion of catalytically-active heteroatoms within the final zeolites achieved through the ADOR method has not been thoroughly demonstrated. This fact precludes the application of these ADORable zeolites as heterogeneous catalysts, and consequently, future research efforts must focus on the development of highly-stable metal-containing ADORable catalysts.

It appears to us that zeolite synthesis and applications is a continuous evolving field full of surprises and potential applications. Just as a very recent example (186), separation of ethene and ethane with an extraordinary selectivity has been achieved with a new pure silica zeolite (ITQ-55), on the bases, not only of pore diameter but also on framework flexibility. This should open new insides on flexibility-assisted molecular diffusions. Finally, new paradigmatic changes in the trinomial zeolite synthesis-structure-reactivity equation, have been put forward by directly preparing zeolite structures that should be adequate for catalyzing predefined particular processes. This can be achieved by starting from the reaction to be catalyzed and establishing its mechanism. Then, a mimic of the reaction transition state is synthesized as an organic structure directing agent (OSDA), and used to prepare the zeolite structure that, by definition, will be able to stabilize the transition state of the desired reaction (14). There is no doubt that the joint development of new synthesis techniques and concepts should help to the synthesis of new zeolite materials while boosting their potential applications.

Acknowledgements

This work has been supported by the Spanish Government-MINECO through “Severo Ochoa” (SEV-2016-0683), and MAT2015-71261-R, by the European Union through

ERC-AdG-2014-671093 (SynCatMatch) and by the Fundación Ramón Areces through a research contract of the “Life and Materials Science” program.

Figure 1. Interzeolite transformation scheme for the zeolite A into hydroxysodalite in alkaline media. Reproduced from reference (47).

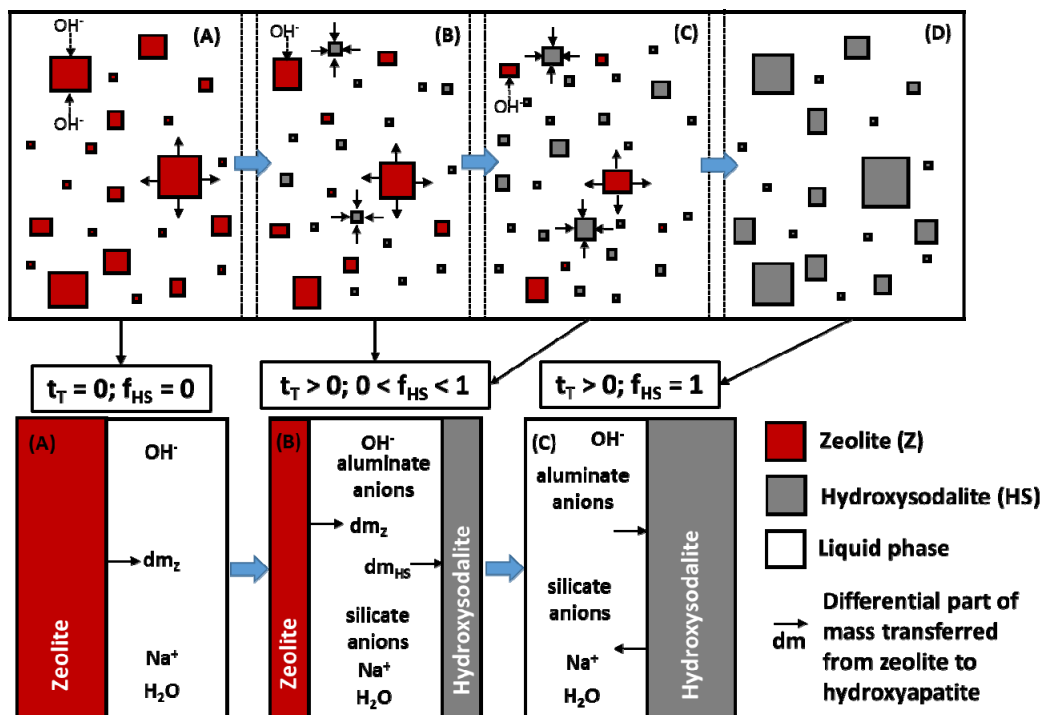


Figure 2. Secondary building units (SBUs) present in different framework structures.

Reproduced from reference (42).

Framework type-code	FAU	*BEA	LEV	MAZ	CHA	GIS	LTL	MOR	FER	MFI
Framework structure										
Composite building unit	 sod	 mor bea d6r	 d6r	 gme	 d6r cha	 gis	 d6r can	 mor	 fer	 mor mel mfi cas

Figure 3. Correlation of common building units for MFI, Beta and MTW. Reproduced from reference (41).

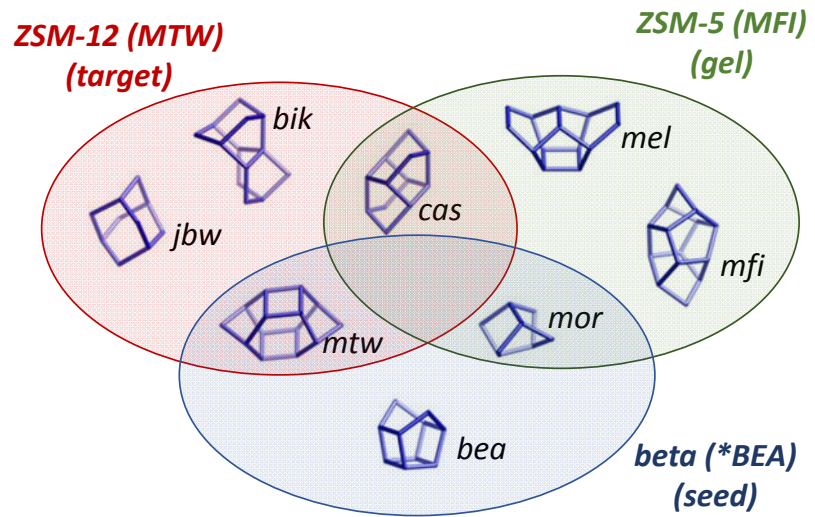


Figure 4. Transformation pathways observed during the Nu-3 crystallization (dashed lines: slow conversion). Reproduced from reference (66).

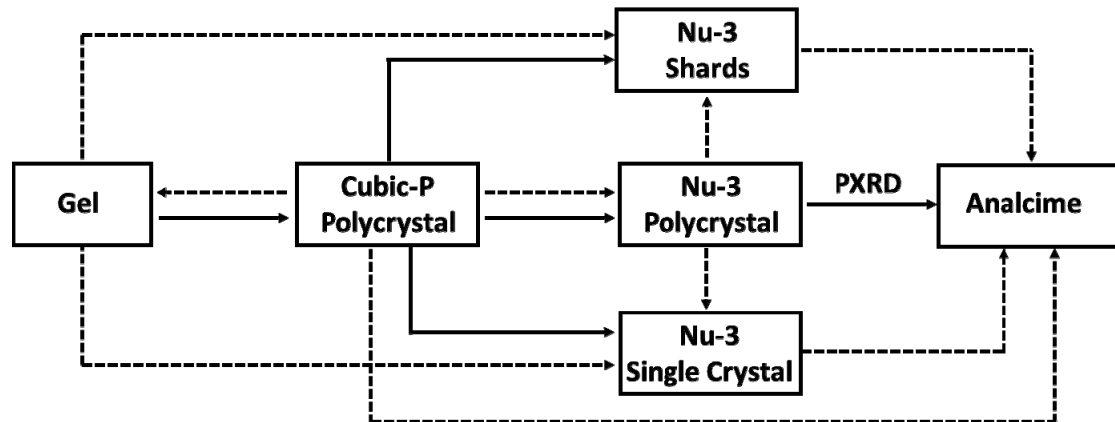


Figure 5. Interzeolite transformation mechanism based on the formation of intermediate locally ordered aluminosilicate species (nanoparts). Reproduced from reference (30).

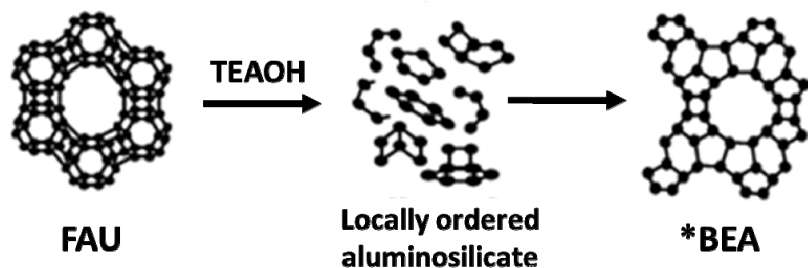


Figure 6. Transformation pathways described for zeolitic layered precursors into different zeolite-based materials through different post-synthetic treatments. Reproduced from (70).

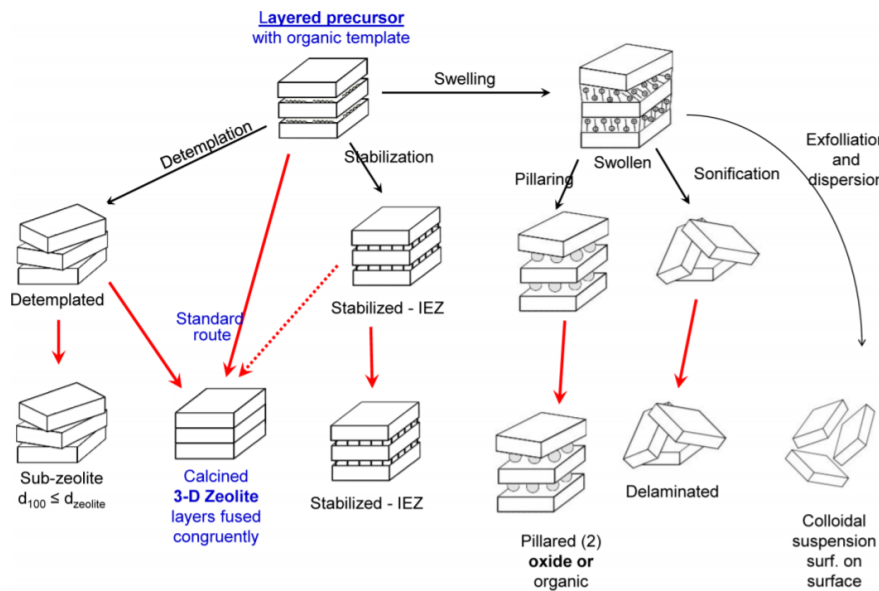


Figure 7. OSDA-free interzeolite transformations to achieve synthetic analogues of rare-earth natural zeolites from GIS-related zeolites (a) and different small pore zeolites from low-silica FAU zeolites (b). Reproduced from (83).

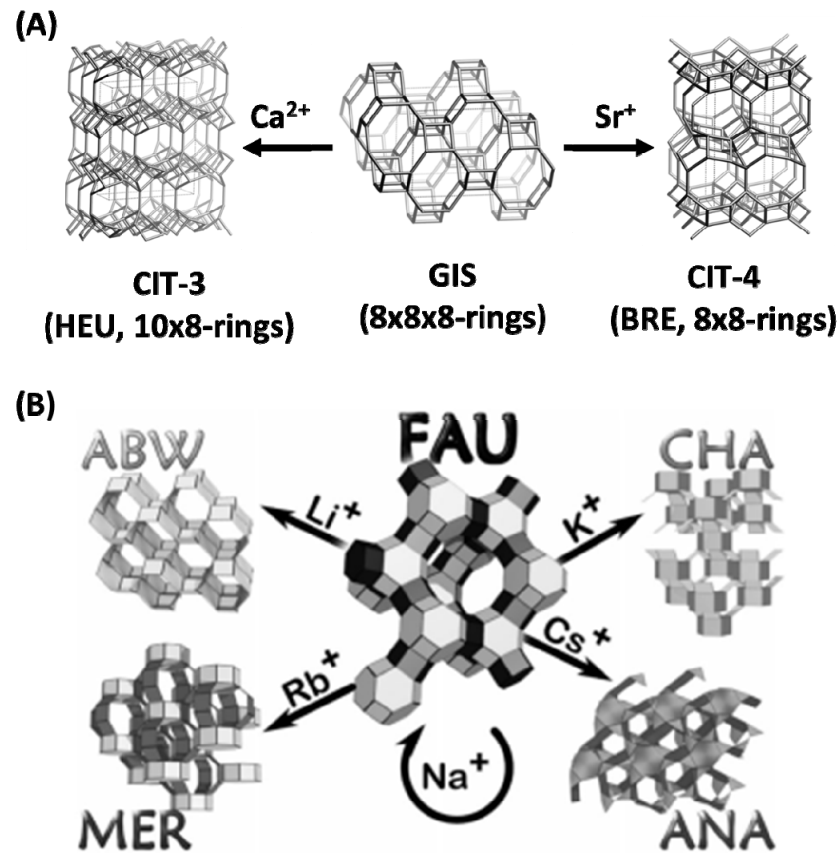


Figure 8. Metal-encapsulation within MFI through OSDA-interzeolite transformation

reported by Iglesia et al. Reproduced from (32).

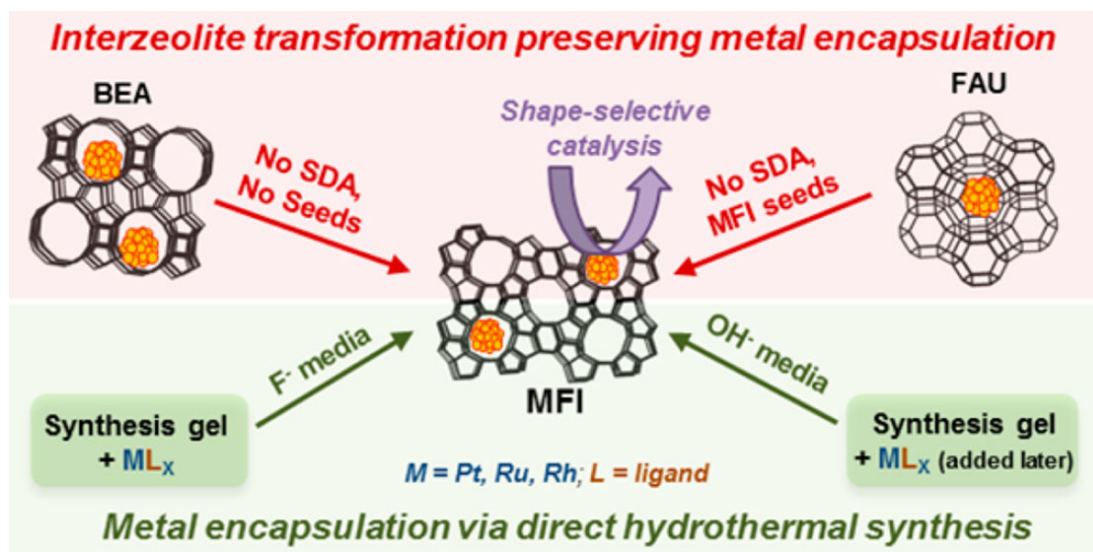


Figure 9. “Green Beta” synthesis. Reproduced from (57).

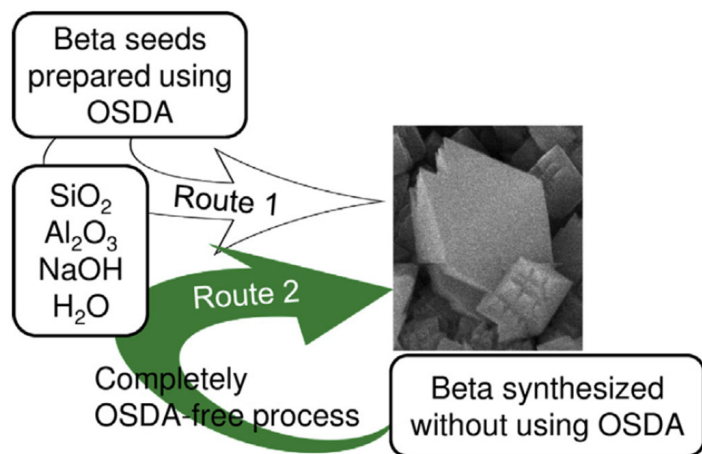


Figure 10. Crystallization of the seed-assisted OSDA-free MWW zeolite. Reproduced from (91).

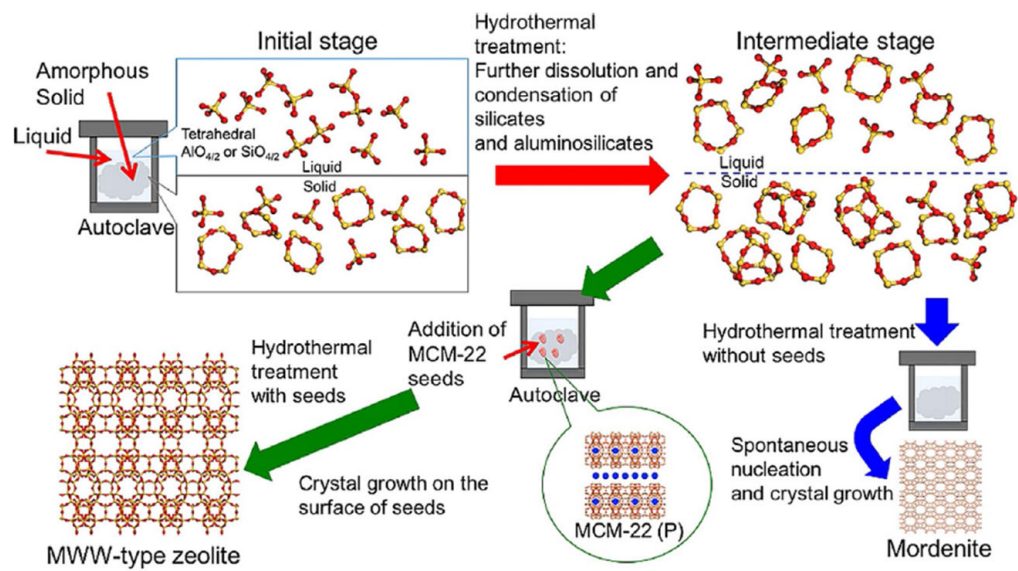


Figure 11. Different OSDA molecules employed for the synthesis of high-silica CHA zeolites through the interzeolite transformation of FAU.

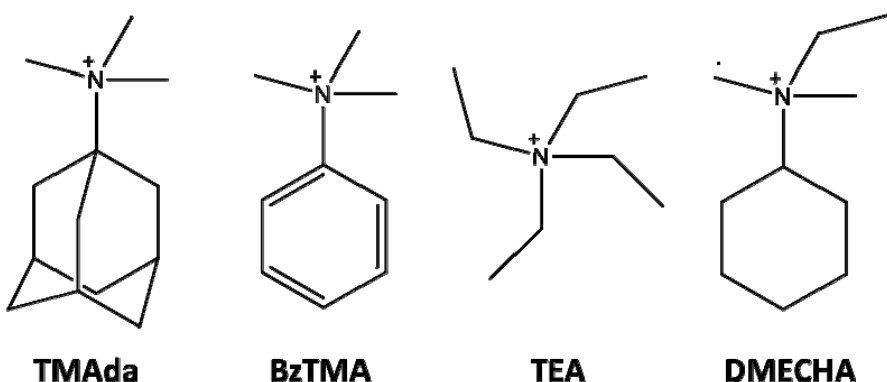


Figure 12. (Left) SEM images of the cross section of a CHA zeolite membrane, and (Right) Long-term testing of CHA zeolite membrane for dehydration of acetic acid solution (50%wt $\text{CH}_3\text{COOH}/\text{H}_2\text{O}$). Reproduced from (101).

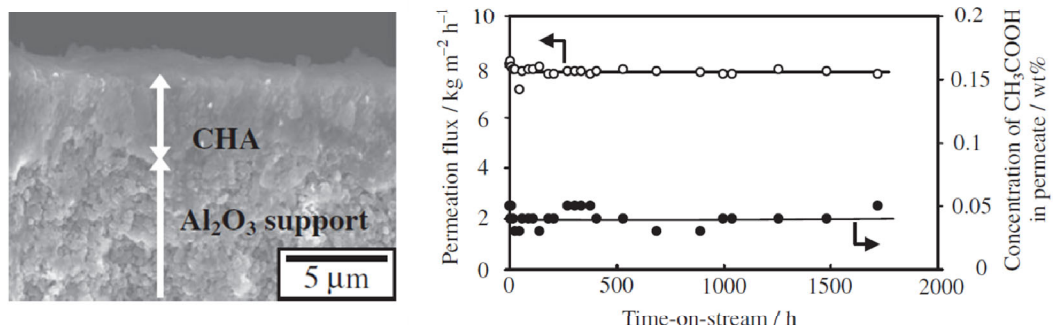


Figure 13. Synthesis methodology proposed by Corma et al. for the FAU transformation into high-silica CHA using TEA as inexpensive OSDA.

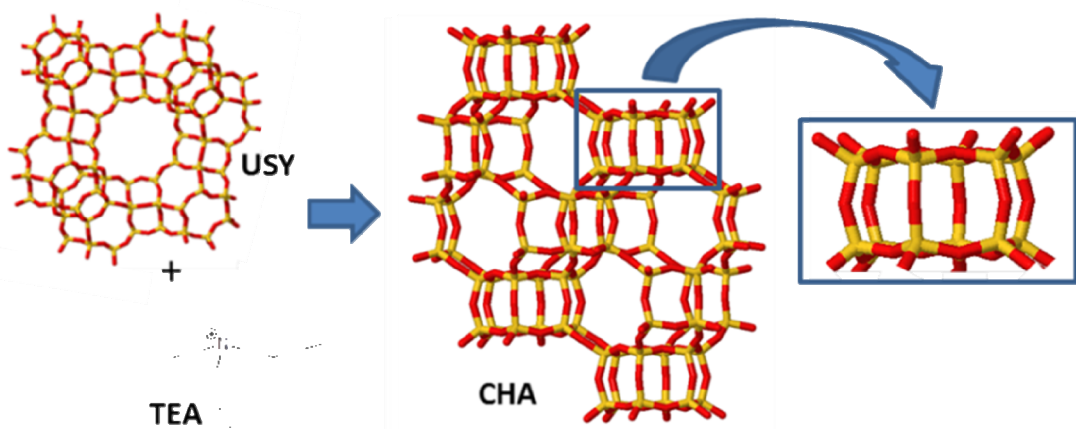


Figure 14. Different OSDA molecules employed for the synthesis of high-silica SSZ-39 zeolite through the interzeolite transformation of FAU.

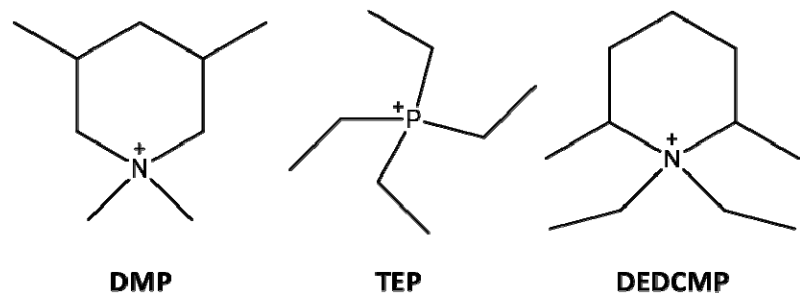


Figure 15. Bulky polycyclic OSDA employed for the synthesis of high-silica ERI and AFX zeolites by interzeolite transformation. Reproduced from (118).

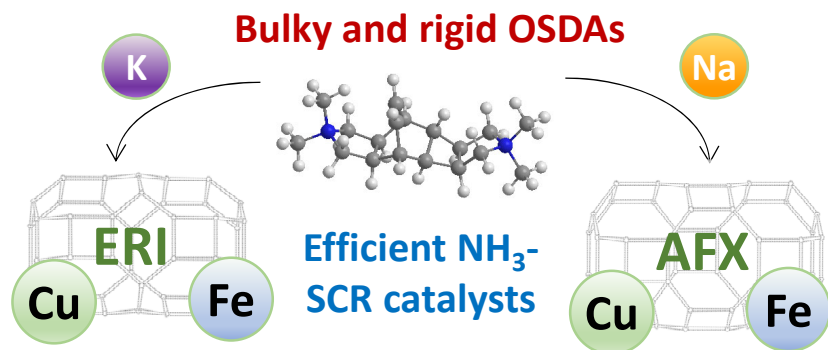


Figure 16. Proposed scheme for the synthesis of mesostructured zeolites combining pre-crystallized zeolites and surfactant-based templates. Reproduced from (133).

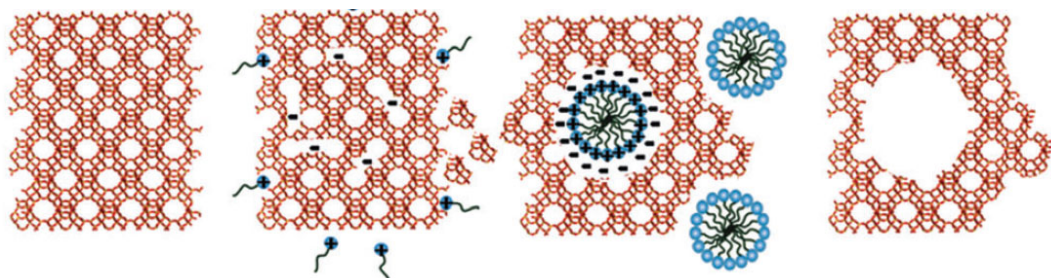


Figure 17. Synthesis pathways reported to achieve different MWW-related materials.

Reproduced from (76).

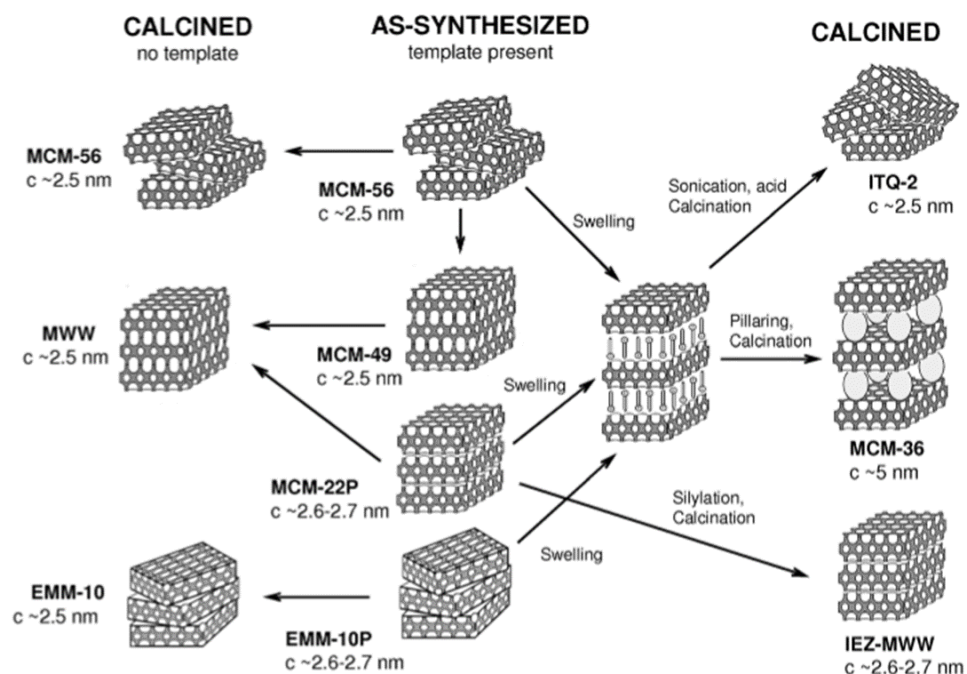


Figure 18. Proposed scheme for the crystallization of ECNU-5 zeolite. Reproduced from (142).

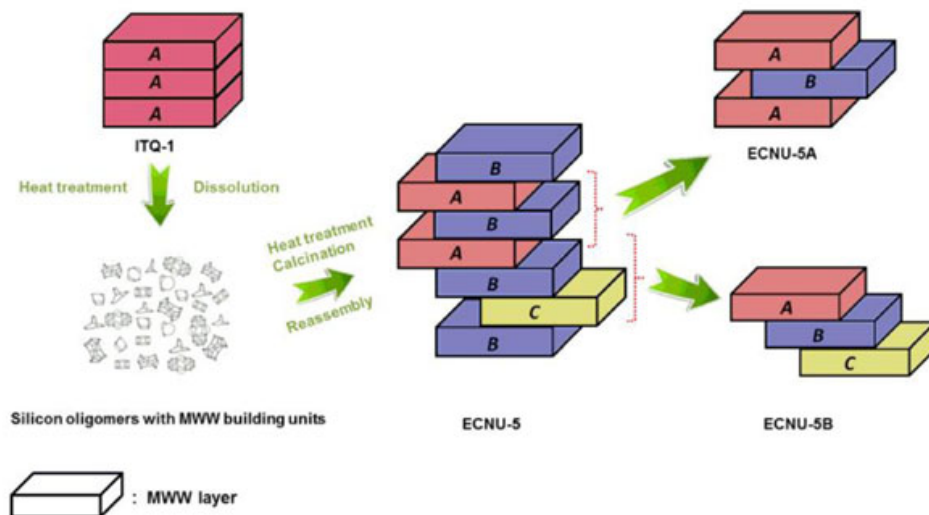


Figure 19. Synthesis methodology followed for the Pt-encapsulated MWW catalyst.

Reproduced from (148).

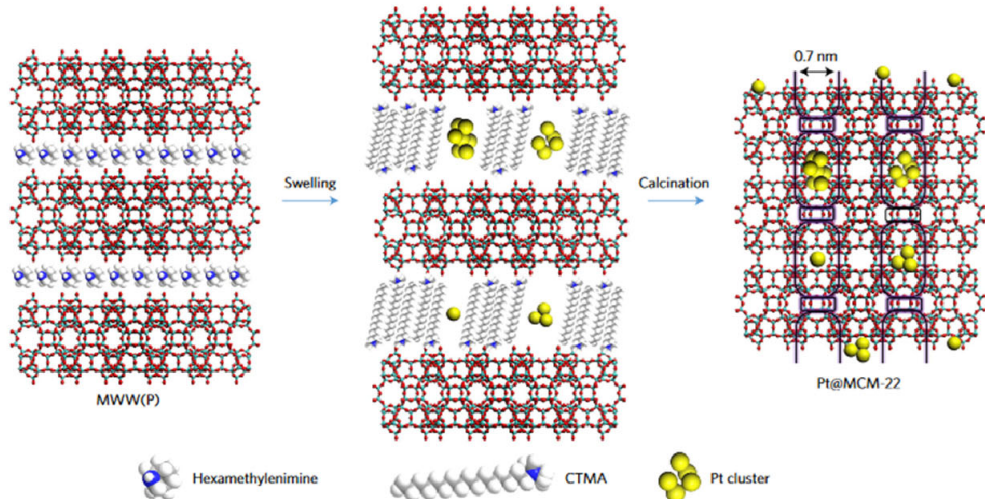


Figure 20. Zeolite synthesis from the layered PREFER precursor. Reproduced from (74).

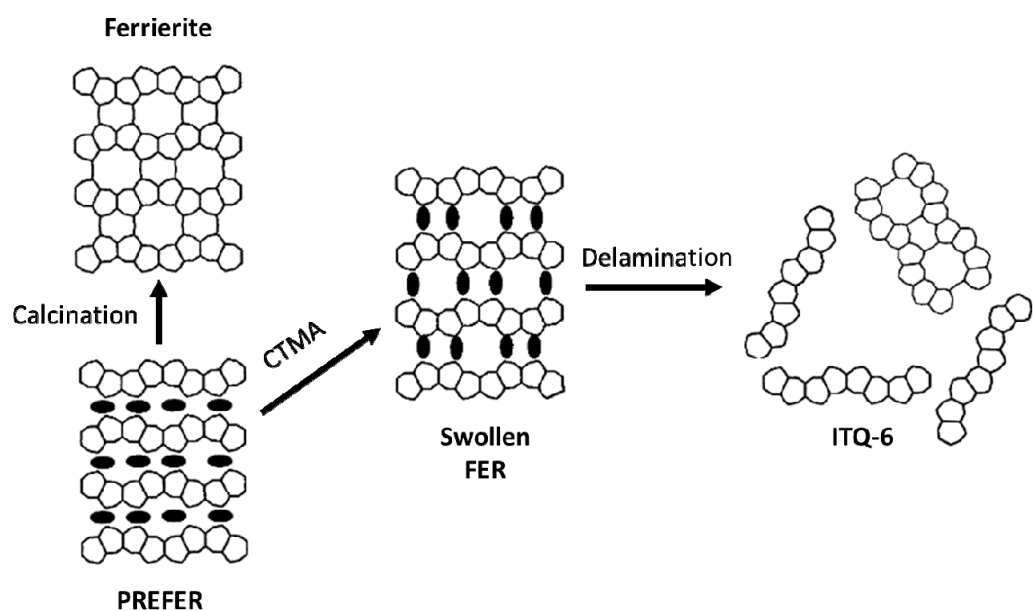


Figure 21. Two possible condensation ways of *fer* layers to form the FER (left) or CDO (right) zeolite frameworks. Reproduced from (157)

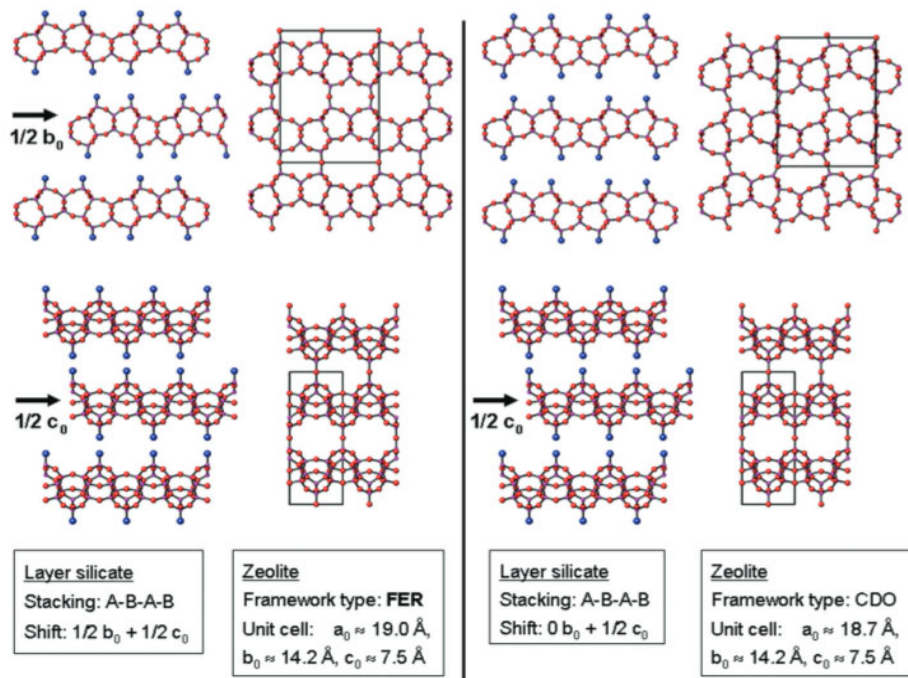


Figure 22. The ADOR (assembly-disassembly-organization-reassembly) methodology.

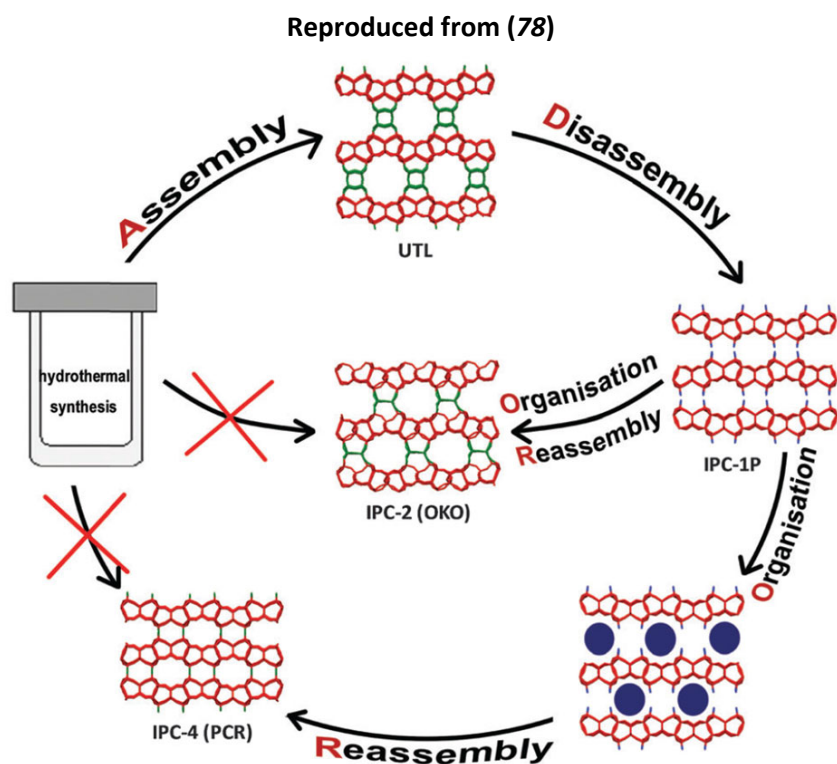


Figure 23. ADOR methodology for the synthesis of new zeolites from the germanosilicate

CFI. Reproduced from (177)

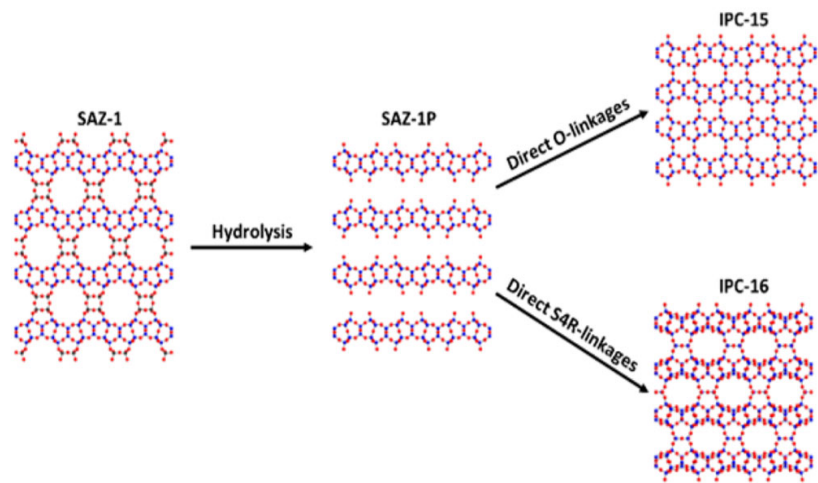


Table 1. Synthesis conditions, product phase and yield of the high-silica MFI samples achieved by interzeolite transformation of Beta or FAU. Reproduced from (26).

sample name	parent zeolite (Si/Al)	NaOH/ SiO ₂ ^b	H ₂ O/ SiO ₂ ^b	time (h)	additional (OSDA/seed) ^c	product phase ^d	product (Si/Al)	final pH	yield ^e (%)
MFI _B -D1	BEA(12.5)	0.35	65	24		Am.			
MFI _B -D2	BEA(37.5)	0.35	65	24		MFI	22	11.8	46
MFI _B -T	BEA(37.5)	0.35	65	24	TPABr (0.05) ^f	MFI	35	12.5	47
MFI _B -S	BEA(37.5)	0.35	65	24	10 wt % MFI seeds	MFI	23	11.8	47
MFI _F -D1	FAU(6)	0.50	95	40		Am.			
MFI _F -D2	FAU(40)	0.50	95	40		Am.			
MFI _F -T	FAU(40)	0.50	95	40	TPABr (0.05) ^f	MFI	33	12.5	58
MFI _F -S1	FAU(40)	0.50	95	40	10 wt % MFI seeds	MFI	22	11.8	47
MFI _F -S2	FAU(40)	0.23	95	40	10 wt % MFI seeds	MFI + Am.	42	11.7	76
MFI _F -S3	FAU(40)	0.85	95	40	10 wt % MFI seeds	MFI	11	12.0	18

^aT = 423 K for all the syntheses. ^bReported values excludes the SiO₂ amount present in seed materials. ^cSeed (wt %) = (seed material (g)/parent zeolite (g)) × 100. ^dAm. = amorphous. ^eYield (%) = [product (g)/(parent zeolite (g) +seed (g))] × 100. ^fValues in parentheses show molar composition of TPABr relative to SiO₂ amount of parent zeolite.

References

1. C. S. Cundy, P. A. Cox, The hydrothermal synthesis of zeolites: Precursors, intermediates and reaction mechanism. *Micropor. Mesopor. Mater.* **82**, 1-78 (2005).
2. C. Martínez, A. Corma, Inorganic molecular sieves: Preparation, modification and industrial application in catalytic processes. *Coord. Chem. Rev.* **255**, 1558-1580 (2011).
3. J. Cejka, G. Centi, J. Perez-Pariente, W. J. Roth, Zeolite-based materials for novel catalytic applications: Opportunities, perspectives and open problems. *Catal. Today* **179**, 2-15 (2012).
4. <http://www.iza-structure.org/databases/>.
5. A. Corma, M. E. Davis, Issues in the synthesis of crystalline molecular sieves: towards the crystallization of low framework-density structures. *ChemPhysChem.* **5**, 304-313 (2004).
6. G. T. Kerr, Chemistry of Crystalline Aluminosilicates. I. Factors Affecting the Formation of Zeolite A. *J. Phys. Chem.* **70**, 1047-1050 (1966).
7. E. G. Derouane, S. Detremmerie, Z. Gabelica, N. Blom, Synthesis and characterization of ZSM-5 type zeolites I. physico-chemical properties of precursors and intermediates. *Appl. Catal.* **1**, 201-224 (1981).
8. C. D. Chang, A. T. Bell, Studies on the mechanism of ZSM-5 formation. *Catal. Lett.* **8**, 305-316 (1991).
9. S. L. Burkett, M. E. Davis, Mechanism of Structure Direction in the Synthesis of Si-ZSM-5: An Investigation by Intermolecular 1H-29Si CP MAS NMR. *J. Phys. Chem.* **98**, 4647 (1994).
10. C. R. A. Catlow, Modelling and Predicting Crystal Structures. *Inter. Sci. Rev.* **40**, 294-307.
11. J. Li, A. Corma, J. Yu, Synthesis of new zeolite structures. *Chem. Soc. Rev.* **44**, 7112-7127 (2015).
12. M. E. Davis, Zeolites from a Materials Chemistry Perspective. *Chem. Mater.* **26**, 239-245 (2014).
13. M. Moliner, C. Martinez, A. Corma, Multipore Zeolites: Synthesis and Catalytic Applications. *Angew. Chem., Int. Ed.* **54**, 3560-3579 (2015).
14. E. M. Gallego *et al.*, "Ab initio" synthesis of zeolites for preestablished catalytic reactions. *Science* **355**, 1051-1055 (2017).
15. R. M. Barrer, P. J. Denny, Hydrothermal chemistry of the silicates. Part IX. Nitrogenous aluminosilicates. *J. Chem. Soc.*, 971-982 (1961).
16. R. F. Lobo, S. I. Zones, M. E. Davis, Structure-direction in zeolite synthesis. *J. Inclusion Phenom. Mol. Recognit. Chem.* **21**, 47-78 (1995).
17. M. Moliner, F. Rey, A. Corma, Towards the Rational Design of Efficient Organic Structure-Directing Agents for Zeolite Synthesis. *Angew. Chem., Int. Ed.* **52**, 13880-13889 (2013).
18. A. W. Burton, S. I. Zones, Organic Molecules in Zeolite Synthesis: Their Preparation and Structure-Directing Effects. *Stud. Surf. Sci. Catal.* **168**, 137-179 (2007).
19. D. L. Dorset *et al.*, P-Derived Organic Cations as Structure-Directing Agents: Synthesis of a High-Silica Zeolite (ITQ-27) with a Two-Dimensional 12-Ring Channel System. *J. Am. Chem. Soc.* **128**, 8862-8867 (2006).
20. R. Simancas *et al.*, Modular Organic Structure-Directing Agents for the Synthesis of Zeolites. *Science* **330**, 1219-1222 (2010).
21. T. Blasco *et al.*, Preferential Location of Ge in the Double Four-Membered Ring Units of ITQ-7

- Zeolite. *J. Phys. Chem. B* **106**, 2634–2642 (2002).
22. A. Corma, M. J. Díaz-Cabañas, F. Rey, S. Nicolopoulus, K. Boulahya, ITQ-15: the first ultralarge pore zeolite with a bi-directional pore system formed by intersecting 14- and 12-ring channels, and its catalytic implications. *Chem. Commun.*, 1356-1357 (2004).
23. A. Corma, M. J. Díaz-Cabañas, J. L. Jordà, C. Martínez, M. Moliner, High-throughput synthesis and catalytic properties of a molecular sieve with 18- and 10-member rings. *Nature* **443**, 842-845 (2006).
24. J. Jiang, Y. J., A. Corma, Extra-Large-Pore Zeolites: Bridging the Gap between Micro and Mesoporous Structures. *Angew. Chem., Int. Ed.* **49**, 3120-3145 (2010).
25. T. Sano, M. Itakura, M. Sadakane, High potential of interzeolite conversion method for zeolite synthesis. *J. Jap. Petrol. Inst.* **56**, 183-197 (2013).
26. S. Goel, S. I. Zones, E. Iglesia, Synthesis of Zeolites via Interzeolite Transformations without Organic Structure-Directing Agents. *Chem. Mater.* **27**, 2056-2066 (2015).
27. N. Martin, M. Moliner, A. Corma, High yield synthesis of high-silica chabazite by combining the role of zeolite precursors and tetraethylammonium: SCR of NOx. *Chem. Commun.* **51**, 9965-9968 (2015).
28. T. Sonoda *et al.*, Synthesis of high-silica AEI zeolites with enhanced thermal stability by hydrothermal conversion of FAU zeolites, and their activity in the selective catalytic reduction of NOx with NH3. *J. Mater. Chem. A* **3**, 857-865 (2015).
29. D. Xie, S. I. Zones, C. M. Lew, T. M. Davis, *WO2016/003504 (2016)*.
30. H. Jon, N. Ikawa, Y. Oumi, T. Sano, An Insight into the Process Involved in Hydrothermal Conversion of FAU to *BEA Zeolite. *Chem. Mater.* **20**, 4135-4141 (2008).
31. I. Goto *et al.*, Transformation of LEV-type zeolite into less dense CHA-type zeolite. *Micropor. Mesopor. Mater.* **158**, 117-122 (2012).
32. S. Goel, S. I. Zones, E. Iglesia, Encapsulation of Metal Clusters within MFI via Interzeolite Transformations and Direct Hydrothermal Syntheses and Catalytic Consequences of Their Confinement. *J. Am. Chem. Soc.* **136**, 15280-15290 (2014).
33. S. I. Zones, Conversion of Faujasites to High-silica Chabazite SSZ-13 in the Presence of N,N,N-Trimethyl-1 -adamantammonium Iodide. *J. Chem. Soc. Faraday Trans.* **87**, 3709-3716 (1991).
34. T. Inoue *et al.*, Synthesis of LEV zeolite by interzeolite conversion method and its catalytic performance in ethanol to olefins reaction. *Micropor. Mesopor. Mater.* **122**, 149-154 (2009).
35. M. Itakura *et al.*, Synthesis of high-silica CHA type zeolite by interzeolite conversion of FAU type zeolite in the presence of seed crystals. *Micropor. Mesopor. Mater.* **144**, 91-96 (2011).
36. N. Martin, C. R. Boruntea, M. Moliner, A. Corma, Efficient synthesis of the Cu-SSZ-39 catalyst for DeNOx applications. *Chem. Commun.* **51**, 11030-11033 (2015).
37. S. Inagaki *et al.*, Rapid synthesis of an aluminum-rich MSE-Type zeolite by the hydrothermal conversion of an FAU-type zeolite. *Chem. Eur. J.* **19**, 7780-7786 (2013).
38. S. I. Zones, Y. Nakagawa, Use of modified zeolites as reagents influencing nucleation in zeolite synthesis. *Stud. Surf. Sci. Catal.* **97**, 45-52 (1995).
39. W. Fan, P. Wu, S. Namba, T. Tatsumi, A Titanosilicate That Is Structurally Analogous to an MWW-Type Lamellar Precursor. *Angew. Chem., Int. Ed.* **43**, 236 -240 (2004).
40. T. De Baerdemaeker *et al.*, From Layered Zeolite Precursors to Zeolites with a Three-Dimensional Porosity: Textural and Structural Modifications through Alkaline

- Treatment. *Chem. Mater.* **27**, 316–326 (2015).
- 41. K. Iyoki, K. Itabashi, T. Okubo, Progress in seed-assisted synthesis of zeolites without using organic structure-directing agents. *Micropor. Mesopor. Mater.* **189**, 22-30 (2014).
 - 42. K. Honda *et al.*, Role of Structural Similarity Between Starting Zeolite and Product Zeolite in the Interzeolite Conversion Process. *J. Nanosci. Nanotech.* **13**, 3020-3026 (2013).
 - 43. R. M. Barrer, Synthesis of a zeolitic mineral with chabazitelike sorptive properties. *J. Chem. Soc.*, 127-132 (1948).
 - 44. R. M. Barrer, D. W. Riley, Sorptive and molecular-sieve properties of a new zeolitic mineral. *J. Chem. Soc.*, 133-143 (1948).
 - 45. R. M. Barrer, J. F. Cole, H. Sticher, Chemistry of soil minerals. V. Low temperature hydrothermal transformations of kaolinite. *J. Chem. Soc. A* **10**, 2475-1485 (1968).
 - 46. D. W. Breck, *Zeolite Molecular Sieves* (Wiley, New York), 1974.
 - 47. B. Subotic, D. Skrtic, I. Smit, Transformation of zeolite A into hydroxysodalite I. An approach to the mechanism of transformation and its experimental evaluation. *J. Cryst. Growth* **50**, 498-508 (1980).
 - 48. B. Subotic, L. Sekovanic, Transformation of zeolite A into hydroxysodalite II. Growth kinetics of hydroxysodalite microcrystals. *J. Cryst. Growth* **75**, 561-572 (1986).
 - 49. B. Subotic, I. Smit, O. Madzija, Kinetic study of the transformation of zeolite A into zeolite P. *Zeolites* **2**, 135-142 (1982).
 - 50. S. Khodabandeh, M. E. Davis, Synthesis of CIT-3: a calcium aluminosilicate with the heulandite topology. *Micropor. Mater.* **9**, 149-160 (1997).
 - 51. S. Khodabandeh, G. Lee, M. E. Davis, CIT-4: The first synthetic analogue of brewsterite. *Micropor. Mater.* **11**, 87-95 (1997).
 - 52. A. Yashiki *et al.*, Hydrothermal conversion of FAU zeolite into LEV zeolite in the presence of non-calcined seed crystals. *J. Cryst. Growth* **325**, 96-100 (2011).
 - 53. K. Honda *et al.*, Influence of seeding on FAU-*BEA interzeolite conversions. *Micropor. Mesopor. Mater.* **142**, 161-167 (2011).
 - 54. G. T. Kerr, Chemistry of crystalline aluminosilicates. IV. Factors affecting the formation of zeolites X and B. *J. Phys. Chem.* **72**, 1385-1386 (1968).
 - 55. B. Xie *et al.*, Organotemplate-Free and Fast Route for Synthesizing Beta Zeolite. *Chem. Mater.* **20**, 4533-4535 (2008).
 - 56. G. Majano, L. Delmotte, V. Valtchev, S. Mintova, Al-rich zeolite beta by seeding in the absence of organic template. *Chem. Mater.* **21**, 4184-4191 (2009).
 - 57. Y. Kamimura, W. Chaikittisilp, K. Itabashi, A. Shimojima, T. Okubo, Critical factors in the seed-assisted synthesis of zeolite beta and "green beta" from OSDA-free Na⁺-aluminosilicate gels. *Chem. Asian J.* **5**, 2182-2191 (2010).
 - 58. B. Xie *et al.*, Seed-directed synthesis of zeolites with enhanced performance in the absence of organic templates. *Chem. Commun.* **47**, 3945-3947 (2011).
 - 59. Y. Kamimura *et al.*, Crystallization Behavior of Zeolite Beta in OSDA-Free, Seed-Assisted Synthesis. *J. Phys. Chem. C* **115**, 744-750 (2011).
 - 60. K. Iyoki, Y. Kamimura, K. Itabashi, A. Shimojima, T. Okubo, Synthesis of MTW-type zeolites in the absence of organic structure-directing agent. *Chem. Lett.* **39**, 730-731 (2010).
 - 61. G. Majano, A. Darwiche, S. Mintova, V. Valtchev, Seed-Induced Crystallization of Nanosized Na-ZSM-5 Crystals. *Ind. Eng. Chem. Res.* **48** **48**, 7084-7091 (2009).

62. H. Zhung *et al.*, Organotemplate-free synthesis of high-silica ferrierite zeolite induced by CDO-structure zeolite building units. *J. Mater. Chem.* **21**, 9494-9497 (2011).
63. T. Yokoi, M. Yoshioka, H. Imai, T. Tatsumi, Diversification of RTH-Type Zeolite and Its Catalytic Application. *Angew. Chem., Int. Ed.* **48**, 9884-9887 (2009).
64. K. Itabashi, Y. Kamimura, K. Iyoki, A. Shimojima, T. Okubo, A Working Hypothesis for Broadening Framework Types of Zeolites in Seed-Assisted Synthesis without Organic Structure-Directing Agent. *J. Am. Chem. Soc.* **134**, 11542-11549 (2012).
65. S. I. Zones, Direct Hydrothermal Conversion of Cubic P Zeolite to Organozeolite SSZ-13. *J. Chem. Soc. Faraday Trans.* **86**, 3467-3472 (1990).
66. I. Y. Chan, S. I. Zones, Analytical electron microscopy (AEM) of Cubic P zeolite to Nu-3 zeolite transformation. *Zeolites* **9**, 3-11 (1989).
67. H. Jon, K. Nakahata, B. Lu, Y. Oumi, T. Sano, Hydrothermal conversion of FAU into *BEA zeolites. *Micropor. Mesopor. Mater.* **96**, 72-78 (2006).
68. H. Jon *et al.*, Effects of structure-directing agents on hydrothermal conversion of FAU type zeolite. *Stud. Surf. Sci. Catal.* **174A**, 229-232 (2008).
69. H. Jon, S. Takahashi, H. Sasaki, Y. Oumi, T. Sano, Hydrothermal conversion of FAU zeolite into RUT zeolite in TMAOH system. *Micropor. Mesopor. Mater.* **113**, 56-63 (2008).
70. W. J. Roth, P. Nachtigall, R. E. Morris, J. Cejka, Two-Dimensional Zeolites: Current Status and Perspectives. *Chem. Rev.* **114**, 4807-4837 (2014).
71. W. J. Roth, C. T. Kresge, J. C. Vartuli, A. S. Fung, S. B. McCullen, MCM-36: The first pillared molecular sieve with zeolite properties. *Stud. Surf. Sci. Catal.* **94**, 301-308 (1995).
72. R. Szostak, *Molecular Sieves: Principles of Synthesis and Identification*; Blackie Academic and Professional: London, 1998.
73. A. Corma, V. Fornés, S. B. Pergher, T. L. M. Maesen, J. G. Buglass, Delaminated zeolite precursors as selective acidic catalysts. *Nature* **396**, 353-356 (1998).
74. A. Corma, U. Díaz, M. E. Domíne, V. Fornés, AlITQ-6 and TiLTQ-6: Synthesis, Characterization, and Catalytic Activity. *Angew. Chem., Int. Ed.* **39**, 1499-1501 (2000).
75. A. Corma, V. Fornés, U. Díaz, ITQ-18 a new delaminated stable zeolite. *Chem. Commun.* **0**, 2642-2643 (2001).
76. W. J. Roth, J. Cejka, Two-dimensional zeolites: dream or reality? *Catal. Sci. Technol.* **1**, 43-53 (2011).
77. C. T. Kresge, W. J. Roth, *U. S. Patent 5266541* (1993).
78. P. Eliasova *et al.*, The ADOR mechanism for the synthesis of new zeolites. *Chem. Soc. Rev.* **44**, 7177-7206 (2015).
79. W. J. Roth *et al.*, A family of zeolites with controlled pore size prepared using a top-down method. *Nat. Chem.* **5**, 628-633 (2013).
80. E. Verheyen *et al.*, Design of zeolite by inverse sigma transformation. *Nat. Mater.* **11**, 1059-1061 (2012).
81. S. Khodabandeh, M. E. Davis, Zeolites P1 and L as precursors for the preparation of alkaline-earth zeolites. *Micropor. Mater.* **12**, 347-359 (1997).
82. S. Khodabandeh, M. E. Davis, Alteration of perlite to calcium zeolites. *Micropor. Mater.* **9**, 161-172 (1997).
83. L. Van Tendeloo, E. Gobechiya, E. Breynaert, J. A. Martens, C. E. A. Kirschhock, Alkaline cations directing the transformation of FAU zeolites into five different framework types. *Chem.*

- Commun.* **49**, 11737-11739 (2013).
- 84. R. Nedyalkova, C. Montreuil, C. Lambert, L. Olsson, Interzeolite Conversion of FAU Type Zeolite into CHA and its Application in NH₃-SCR. *Top. Catal.* **56**, 550-557 (2013).
 - 85. Y. Ji, M. A. Deimund, Y. Bhawe, M. E. Davis, Organic-Free Synthesis of CHA-Type Zeolite Catalysts for the Methanol-to-Olefins Reaction. *ACS Catal.* **5**, 4456-4465 (2015).
 - 86. D. Xie, *WO2016/122724* (2016).
 - 87. R. H. Daniels, G. T. Kerr, L. D. Rollmann, Cationic polymers as templates in zeolite crystallization. *J. Am. Chem. Soc.* **100**, 3097-3100 (1978).
 - 88. K. Honda, A. Yashiki, M. Sadakane, T. Sano, Hydrothermal conversion of FAU and /BEA-type zeolites into MAZ-type zeolites in the presence of non-calcined seed crystals. *Micropor. Mesopor. Mater.* **196**, 254-260 (2014).
 - 89. T. De Baerdemaeker *et al.*, Catalytic applications of OSDA-free Beta zeolite. *J. Catal.* **308**, 73-81 (2013).
 - 90. Y. Kamimura, K. Itabashi, T. Okubo, Seed-assisted, OSDA-free synthesis of MTW-type zeolite and “Green MTW” from sodium aluminosilicate gel systems. *Micropor. Mesopor. Mater.* **147**, 149-156 (2012).
 - 91. Y. Kamimura, K. Itabashi, Y. Kon, A. Endo, T. Okubo, Seed-Assisted Synthesis of MWW-Type Zeolite with Organic Structure-Directing Agent-Free Na-Aluminosilicate Gel System. *Chem. Asian J.* **12**, 530-542 (2017).
 - 92. M. Moliner, C. Martinez, A. Corma, Synthesis Strategies for Preparing Useful Small Pore Zeolites and Zeotypes for Gas Separations and Catalysis. *Chem. Mater.* **26**, 246-258 (2014).
 - 93. H. Zhang *et al.*, Organotemplate-free and seed-directed synthesis of levyne zeolite. *Micropor. Mesopor. Mater.* **155**, 1-7 (2012).
 - 94. H. Imai, N. Hayashida, T. Yokoi, T. Tatsumi, Direct crystallization of CHA-type zeolite from amorphous aluminosilicate gel by seed-assisted method in the absence of organic-structure-directing agents. *Micropor. Mesopor. Mater.* **196**, 341-348 (2014).
 - 95. F. G. Dwyer, P. Chu, ZSM-4 Crystallization via Faujasite Metamorphosis *J. Catal.* **59**, 263-271 (1979).
 - 96. A. J. Perrotta, C. Kibby, B. R. Mitchell, E. R. Tucci, The synthesis, characterization, and catalytic activity of omega and ZSM-4 zeolites. *J. Catal.* **55**, 240-249 (1978).
 - 97. S. I. Zones, *US 4544538* (1985).
 - 98. S. I. Zones, R. A. Van Nordstrand, Novel zeolite transformations: The template-mediated conversion of Cubic P zeolite to SSZ-13. *Zeolites* **8**, 166-174 (1988).
 - 99. M. Itakura *et al.*, Synthesis of High-silica CHA Zeolite from FAU Zeolite in the Presence of Benzyltrimethylammonium Hydroxide. *Chem. Lett.* **37**, 908-909 (2008).
 - 100. N. Yamanaka *et al.*, Acid stability evaluation of CHA-type zeolites synthesized by interzeolite conversion of FAU-type zeolite and their membrane application for dehydration of acetic acid aqueous solution. *Micropor. Mesopor. Mater.* **158**, 141-147 (2012).
 - 101. N. Yamanaka, M. Itakura, Y. Kiyozumi, M. Sadakane, T. Sano, Effect of Structure-Directing Agents on FAU-CHA Interzeolite Conversion and Preparation of High Pervaporation Performance CHA Zeolite Membranes for the Dehydration of Acetic Acid Solution. *Bull. Chem. Soc. Jpn.* **86**, 1333-1340 (2013).
 - 102. T. Takata, N. Tsunogi, Y. Takamitsu, M. Sadakane, T. Sano, Nanosized CHA zeolites with high thermal and hydrothermal stability derived from the hydrothermal conversion of FAU zeolite.

- Micropor. Mesopor. Mater.* **225**, 524-533 (2016).
103. N. Martin, P. N. R. Vennestrom, J. R. Thogersen, M. Moliner, A. Corma, Fe-Containing Zeolites for NH₃-SCR of NO_x: Effect of Structure, Synthesis Procedure, and Chemical Composition on Catalytic Performance and Stability. *Chem. Eur. J.* DOI: **10.1002/chem.201701742**, (2017).
104. X. Xiong *et al.*, Efficient and rapid transformation of high silica CHA zeolite from FAU zeolite in the absence of water solvent. *J. Mater. Chem. A* DOI: **10.1039/C7TA01749A** (2017).
105. T. Takata, N. Tsunogi, Y. Takamitsu, M. Sadakane, T. Sano, Incorporation of various heterometal atoms in CHA zeolites by hydrothermal conversion of FAU zeolite and their performance for selective catalytic reduction of NO_x with ammonia. *Micropor. Mesopor. Mater.* **246**, 89-101 (2017).
106. Y. Kunitake *et al.*, Synthesis of titanated chabazite with enhanced thermal stability by hydrothermal conversion of titanated faujasite. *Micropor. Mesopor. Mater.* **215**, 58-66 (2015).
107. H. Sasaki *et al.*, Hydrothermal conversion of FAU zeolite into aluminous MTN zeolite. *J. Porous Mater.* **16**, 465-471 (2009).
108. S. Shibata, M. Itakura, Y. Ide, M. Sadakane, T. Sano, FAU-LEV interzeolite conversion in fluoride media. *Micropor. Mesopor. Mater.* **138**, 32-39 (2011).
109. T. M. Davis, US9156706 (2015).
110. M. Moliner, C. Franch, E. Palomares, M. Grill, A. Corma, Cu-SSZ-39, an active and hydrothermally stable catalyst for the selective catalytic reduction of NO_x. *Chem. Commun.* **48**, 8264-8266 (2012).
111. M. Dusselier, M. A. Deimund, J. E. Schmidt, M. E. Davis, Methanol-to-Olefins Catalysis with Hydrothermally Treated Zeolite SSZ-39. *ACS Catal.* **5**, 6078-6085 (2015).
112. S. I. Zones, Y. Nakagawa, S. T. Evans, G. S. Lee, US 5958370 (1999).
113. P. Wagner *et al.*, Guest/Host Relationships in the Synthesis of the Novel Cage-Based Zeolites SSZ-35, SSZ-36, and SSZ-39. *J. Am. Chem. Soc.* **122**, 263-273 (2000).
114. Y. Nakagawa, S. Inagaki, Y. Kubota, Direct Hydrothermal Synthesis of High-silica SSZ-39 Zeolite with Small Particle Size. *Chem. Lett.* **45**, 919-921 (2016).
115. B. N. Bhadra *et al.*, Syntheses of SSZ-39 and mordenite zeolites with N,N-dialkyl-2,6-dimethyl-piperidinium hydroxide/iodides: Phase-selective syntheses with anions. *Micropor. Mesopor. Mater.* **235**, 135-142 (2016).
116. N. Martin, P. N. R. Vennestrom, J. R. Thogersen, M. Moliner, A. Corma, Iron-Containing SSZ-39 (AEI) Zeolite: An Active and Stable High-Temperature NH₃-SCR Catalyst. *ChemCatChem* **9**, 1754-1757 (2017).
117. N. Martin *et al.*, Nanocrystalline SSZ-39 zeolite as an efficient catalyst for the methanol-to-olefin (MTO) process. *Chem. Commun.* **52**, 6072-6075 (2016).
118. N. Martín *et al.*, Cage-based small-pore catalysts for NH₃-SCR prepared by combining bulky organic structure directing agents with modified zeolites as reagents. *Appl. Catal. B* **217**, 125-136 (2017).
119. M. Itakura, Y. Oumi, M. Sadakane, T. Sano, Synthesis of high-silica offretite by the interzeolite conversion method. *Mater. Res. Bull.* **45**, 646-650 (2010).
120. Y. Kubota *et al.*, Remarkable enhancement of catalytic activity and selectivity of MSE-type zeolite by post-synthetic modification. *Catal. Today* **243**, 85-91 (2015).
121. Y. Shi *et al.*, Topology reconstruction from FAU to MWW structure. *Micropor. Mesopor. Mater.* **200**, 267-278 (2014).

122. J. E. Schmidt, C. Y. Chen, S. K. Brand, S. I. Zones, M. E. Davis, Facile Synthesis, Characterization, and Catalytic Behavior of a Large-Pore Zeolite with the IWW Framework. *Chem. Eur. J.* **22**, 4022-4029 (2016).
123. S. I. Zones, Y. Nakagawa, Boron-beta zeolite hydrothermal conversions: the influence of template structure and of boron concentration and source *Micropor. Mater.* **2**, 543-555 (1994).
124. H. Maekawa, Y. Kubota, Y. Sug, Hydrothermal Synthesis of [Al]-SSZ-24 from [Al]-Beta Zeolite ([Al]-BEA) as Precursors. *Chem. Lett.* **33**, 1126-1127 (2004).
125. R. K. Ahedi, Y. Kubota, Y. Sugi, Hydrothermal synthesis of [Al]-SSZ-31 from [Al]-BEA precursors. *J. Mater. Chem.* **11**, 2922-2924 (2001).
126. Y. Kubota, H. Maekawa, S. Miyata, T. Tatsumi, Y. Sugi, Hydrothermal synthesis of metallosilicate SSZ-24 from metallosilicate beta as precursors. *Micropor. Mesopor. Mater.* **101**, 115-126 (2007).
127. J. S. Beck, J. C. Vartuli, W. J. Roth, M. E. Leonowicz, C. T. Kresge, Ordered mesoporous molecular sieves synthesized by a liquid-crystal template mechanism. *Nature* **359**, 710-712 (1992).
128. J. S. Beck *et al.*, A New Family of Mesoporous Molecular Sieves Prepared with Liquid Crystal Templates. *J. Am. Chem. Soc.* **114**, 10834-10843 (1992).
129. A. Corma, From Microporous to Mesoporous Molecular Sieve Materials and Their Use in Catalysis. *Chem. Rev.* **97**, 2373-2420 (1997).
130. Y. Tao, H. Kanoh, L. Abrams, K. Kaneko, Mesopore-Modified Zeolites: Preparation, Characterization, and Applications. *Chem. Rev.* **106**, 896-910 (2006).
131. T. Prasomsri, W. Jiao, S. Z. Wenga, J. Garcia-Martinez, Mesostructured zeolites: bridging the gap between zeolites and MCM-41. *Chem. Commun.* **51**, 8900-8911 (2015).
132. R. Chal, T. Cacciaguerra, S. van Donk, C. Gérardin, Pseudomorphic synthesis of mesoporous zeolite Y crystals. *Chem. Commun.* **46**, 7840-7842 (2010).
133. J. Garcia-Martinez, M. Johnson, J. Valla, K. Li, J. Y. Ying, Mesostructured zeolite Y-high hydrothermal stability and superior FCC catalytic performance. *Catal. Sci. Technol.* **2**, 987-994 (2012).
134. S. Liu *et al.*, Preformed zeolite precursor route for synthesis of mesoporous X zeolite. *Colloids Surf. A* **318**, 269-274 (2008).
135. U. Díaz, A. Corma, Layered zeolitic materials: an approach to designing versatile functional solids. *Dalton Trans.* **43**, 10292-10316 (2014).
136. U. Díaz, Layered Materials with Catalytic Applications: Pillared and Delaminated Zeolites from MWW Precursors. *ISRN Chem. Eng. Article ID 537164*, 35 pp (2012).
137. M. E. Leonowicz, J. A. Lawton, S. L. Lawton, M. K. Rubin, MCM-22: A molecular sieve with two independent multidimensional channel systems. *Science* **264**, 1910-1913 (1994).
138. S. L. Lawton *et al.*, Zeolite MCM-49: A Three-Dimensional MCM-22 Analogue Synthesized by in Situ Crystallization. *J. Phys. Chem.* **100**, 3788-3798 (1996).
139. A. Corma, U. Díaz, T. García, G. Sastre, A. Velty, Multifunctional Hybrid Organic-Inorganic Catalytic Materials with a Hierarchical System of Well-Defined Micro- and Mesopores. *J. Am. Chem. Soc.* **132**, 15011-15021 (2010).
140. A. Corma *et al.*, Characterization and Catalytic Activity of MCM-22 and MCM-56 Compared with ITQ-2. *J. Catal.* **191**, 218-224 (2000).

141. M. A. Camblor, A. Corma, M. J. Diaz-Cabanas, C. Baerlocher, Synthesis and Structural Characterization of MWW Type Zeolite ITQ-1, the Pure Silica Analog of MCM-22 and SSZ-25. *J. Phys. Chem. B* **102**, 44-51 (1998).
142. L. Xu *et al.*, Intergrown Zeolite MWW Polymorphs Prepared by the Rapid Dissolution-Recrystallization Route. *Chem. Mater.* **27**, 7852-7860 (2015).
143. A. Corma, U. Díaz, M. E. Domíne, V. Fornés, New Aluminosilicate and Titanosilicate Delaminated Materials Active for Acid Catalysis, and Oxidation Reactions Using H₂O₂. *J. Am. Chem. Soc.* **122**, 2804-2809 (2000).
144. M. Osman, S. Al-Khattaf, U. Díaz, C. Martínez, A. Corma, Influencing the activity and selectivity of alkylaromatic catalytic transformations by varying the degree of delamination in MWW zeolites. *Catal. Sci. Technol.* **6**, 3166-3181 (2016).
145. I. Rodriguez, M. J. Climent, S. Iborra, V. Fornés, A. Corma, Use of Delaminated Zeolites (ITQ-2) and Mesoporous Molecular Sieves in the Production of Fine Chemicals: Preparation of Dimethylacetals and Tetrahydropyranylation of Alcohols and Phenols. *J. Catal.* **192**, 441-447 (2000).
146. A. Corma *et al.*, Preparation, characterisation and catalytic activity of ITQ-2, a delaminated zeolite. *Micropor. Mesopor. Mater.* **38**, 301-309 (2000).
147. A. Corma *et al.*, Ti/ITQ-2, a new material highly active and selective for the epoxidation of olefins with organic hydroperoxides. *Chem. Commun.*, 779-780 (1999).
148. L. Liu *et al.*, Generation of subnanometric platinum with high stability during transformation of a 2D zeolite into 3D. *Nat. Mater.* **16**, 132-138 (2017).
149. W. S. Wise, R. W. Tschernich, Chemical composition of ferrierite. *Am. Mineral.* **61**, 60-65 (1976).
150. H. Gies, R. P. Gunawardane, One-step synthesis, properties and crystal structure of aluminium-free ferrierite. *Zeolites* **7**, 442-445 (1987).
151. L. Schreyeck, P. Caullet, J. C. Mougenel, J. L. Guth, B. Marler, PREFER: a new layered (alumino)silicate precursor of FER-type zeolite *Micropor. Mater.* **6**, 259-271 (1996).
152. T. Ikeda, S. Kayamori, F. Mizukami, Synthesis and crystal structure of layered silicate PLS-3 and PLS-4 as a topotactic zeolite precursor. *J. Mater. Chem.* **19**, 5518-5525 (2009).
153. B. Yang *et al.*, Selective skeletal isomerization of 1-butene over FER-type zeolites derived from PLS-3 lamellar precursors. *Appl. Catal. A* **455**, 107-113 (2013).
154. A. W. Burton, R. J. Accardi, R. F. Lobo, M. Falconi, M. W. Deem, MCM-47: A Highly Crystalline Silicate Composed of Hydrogen-Bonded Ferrierite Layers. *Chem. Mater.* **12**, 2936-2942 (2000).
155. A. Corma, U. Díaz, V. Fornés, *WO2002060815* (2002).
156. A. Chica, U. Díaz, V. Fornés, A. Corma, Changing the hydroisomerization to hydrocracking ratio of long chain alkanes by varying the level of delamination in zeolitic (ITQ-6) materials. *Catal. Today* **147**, 179-185 (2009).
157. B. Marler, Y. Wang, J. Song, H. Gies, Topotactic condensation of layer silicates with ferrierite-type layers forming porous tectosilicates. *Dalton Trans.* **43**, 10396-10416 (2014).
158. D. L. Dorset, G. J. Kennedy, Crystal Structure of MCM-65: An Alternative Linkage of Ferrierite Layers. *J. Phys. Chem. B* **108**, 15216-15222 (2004).
159. T. Ikeda, Y. Akiyama, Y. Oumi, A. Kawai, F. Mizukami, The topotactic conversion of a novel layered silicate into a new framework zeolite. *Angew. Chem., Int. Ed.* **43**, 4892-4896 (2004).

160. N. Tsunooji, T. Ikeda, Y. Ide, M. Sadakane, T. Sano, Synthesis and characteristics of novel layered silicates HUS-2 and HUS-3 derived from a SiO₂-choline hydroxide-NaOH-H₂O system. *J. Mater. Chem.* **22**, 13682-13690 (2012).
161. P. Wu *et al.*, Methodology for Synthesizing Crystalline Metallosilicates with Expanded Pore Windows Through Molecular Alkoxysilylation of Zeolitic Lamellar Precursors. *J. Am. Chem. Soc.* **130**, 8178-8187 (2008).
162. R. Martínez-Franco, C. Paris, J. Martínez-Triguero, M. Moliner, A. Corma, Direct synthesis of the aluminosilicate form of the small pore CDO zeolite with novel OSDAs and the expanded polymorphs. *Micropor. Mesopor. Mater.* **246**, 147-157 (2017).
163. T. V. Whittam, *US Pat*, 4397825 (1983).
164. S. Zanardi *et al.*, Crystal Structure Determination of Zeolite Nu-6(2) and Its Layered Precursor Nu-6(1). *Angew. Chem., Int. Ed.* **43**, 4933-4937 (2004).
165. S. J. Andrews *et al.*, Piperazine Silicate (EU-19)-The structure of a very small crystal determined with synchrotron radiation. *Acta Cryst. B* **44**, 73-77 (1988).
166. B. Marler, M. A. Camblor, H. Gies, The disordered structure of silica zeolite EU-20b, obtained by topotactic condensation of the piperazinium containing layer silicate EU-19. *Micropor. Mesopor. Mater.* **90**, 87-101 (2006).
167. J. Sun *et al.*, The ITQ-37 mesoporous chiral zeolite. *Nature* **458**, 1154-1157 (2009).
168. J. L. Paillaud, B. Harbuzaru, J. Partarin, N. Bats, Extra-Large-Pore Zeolites with Two-Dimensional Channels Formed by 14 and 12 Rings. *Science* **304**, 990-992 (2004).
169. W. J. Roth *et al.*, Postsynthesis Transformation of Three-Dimensional Framework into a Lamellar Zeolite with Modifiable Architecture. *J. Am. Chem. Soc.* **133**, 6130-6133 (2011).
170. N. Kasian *et al.*, NMR Evidence for Specific Germanium Siting in IM-12 Zeolite. *Chem. Mater.* **26**, 5556-5565 (2014).
171. A. Corma, F. Rey, S. Valencia, J. L. Jorda, J. Rius, A zeolite with interconnected 8-, 10- and 12-ring pores and its unique catalytic selectivity. *Nat. Mater.* **2**, 493-497 (2003).
172. R. Castañeda, A. Corma, V. Fornés, F. Rey, J. Rius, Synthesis of a New Zeolite Structure ITQ-24, with Intersecting 10- and 12-Membered Ring Pores. *J. Am. Chem. Soc.* **125**, 7820-7821 (2003).
173. A. Corma, M. Puche, F. Rey, G. Sankar, S. J. Teat, A Zeolite Structure (ITQ-13) with Three Sets of Medium-Pore Crossing Channels Formed by 9- and 10-Rings. *Angew. Chem., Int. Ed.* **115**, 1188–1191 (2003).
174. M. Mazur, P. Chlubná-Eliásová, W. J. Roth, J. Cejka, Intercalation chemistry of layered zeolite precursor IPC-1P. *Catal. Today* **227**, 37-44 (2014).
175. P. Chlubna-Eliasova *et al.*, The Assembly-Disassembly-Organization-Reassembly Mechanism for 3D-2D-3D Transformation of Germanosilicate IWW Zeolite. *Angew. Chem., Int. Ed.* **126**, 7168-7172 (2014).
176. V. Kasneryk *et al.*, Expansion of the ADOR Strategy for the Synthesis of Zeolites: The Synthesis of IPC-12 from Zeolite UOV. *Angew. Chem., Int. Ed.* **56**, 4324-4327 (2017).
177. D. S. Firth *et al.*, Assembly-Disassembly-Organization-Reassembly Synthesis of Zeolites Based on cfi-Type Layers. *Chem. Mater.* **29**, 5605-5611 (2017).
178. S. I. Zones, Translating new materials discoveries in zeolite research to commercial manufacture. *Micropor. Mesopor. Mater.* **144**, 1-8 (2011).
179. B. C. Gates, M. Flytzani-Stephanopoulos, D. A. Dixon, A. Katz, Atomically dispersed supported metal catalysts: perspectives and suggestions for future research. *Catal. Sci. Technol.* **7**,

- 4259-4275 (2017).
180. P. Tomkins, M. Ranocchiari, J. A. van Bokhoven, Direct Conversion of Methane to Methanol under Mild Conditions over Cu-Zeolites and beyond. *Acc. Chem. Res.* **50**, 418–425 (2017).
181. A. M. Beale, F. Gao, I. Lezcano-Gonzalez, C. H. F. Pedenc, J. Szanyi, Recent advances in automotive catalysis for NO_x emission control by small-pore microporous materials. *Chem. Soc. Rev.* **44**, 7371-7405 (2015).
182. M. Moliner, A. Corma, General Aspects on Structure and Reactivity of Framework and Extra-framework Metals in Zeolite Materials. *Struct. Bond.* DOI: [10.1007/430_2017_21](https://doi.org/10.1007/430_2017_21), (2018).
183. A. W. Burton, *WO2014/099261* (2014).
184. R. Martinez-Franco *et al.*, High-silica nanocrystalline Beta zeolites: efficient synthesis and catalytic application. *Chem. Sci.* **7**, 102-108 (2016).
185. E. M. Gallego *et al.*, Simple organic structure directing agents for synthesizing nanocrystalline zeolites. *Chem. Sci.* **8**, 8138-8149 (2017).
186. P. J. Berceciartua *et al.*, Control of zeolite framework flexibility and pore topology for separation of ethane and ethylene. *Science* **358**, 1068-1071 (2017).